

1 **Microbial diversity and abundance vary along salinity,**  
2 **oxygen and particle size gradients in the Chesapeake**  
3 **Bay**

4  
5

6 **Authors**

7

8 Jacob A. Cram<sup>1\*</sup>, Ashley Hollins<sup>1</sup>, Alexandra J. McCarty<sup>1,2</sup>, Grace Martinez<sup>3</sup>, Minming Cui<sup>4</sup>,  
9 Maya L. Gomes<sup>4</sup>, Clara A. Fuchsman<sup>1</sup>

10

11 <sup>1</sup>University of Maryland Center for Environmental Science - Horn Point Laboratory

12 Cambridge, Maryland, United States

13 <sup>2</sup> Virginia Institute of Marine Science - Marine Advisory Program; Gloucester, Virginia, United  
14 States

15 <sup>3</sup>Maryland Sea Grant College, College Park, MD 20740

16 <sup>4</sup>Johns Hopkins University - Earth and Planetary Sciences; Baltimore, Maryland, United States

17

18 \*Correspondence: [jcram@umces.edu](mailto:jcram@umces.edu)

19 **Abstract**

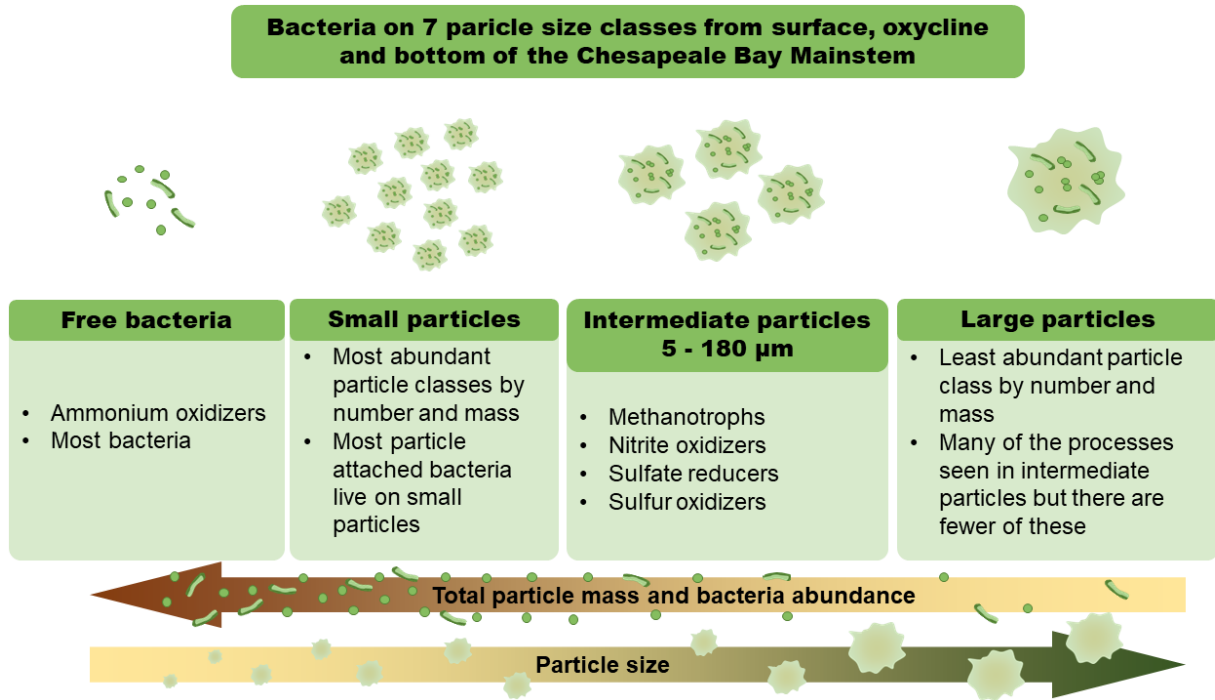
20 Marine snow and other particles are abundant in estuaries, where they drive biogeochemical  
21 transformations and elemental transport. Particles range in size, thereby providing a  
22 corresponding gradient of habitats for marine microorganisms. We used standard normalized  
23 amplicon sequencing, verified with microscopy, to characterize taxon-specific microbial  
24 abundances, (cells per liter of water and per mg of particles), across six particle size classes,  
25 ranging from 0.2 to 500  $\mu\text{m}$ , along the main stem of the Chesapeake Bay estuary. Microbial  
26 communities varied with salinity, oxygen concentrations and particle size. Many taxonomic  
27 groups were most densely packed on large particles (in cells/mg particles), yet were primarily  
28 associated with the smallest particle size class, because small particles made up a substantially  
29 larger portion of total particle mass. However, organisms potentially involved in methanotrophy,  
30 nitrite oxidation, and sulfate reduction were found primarily on intermediately sized (5 - 180  $\mu\text{m}$ )  
31 particles, where species richness was also highest. All abundant ostensibly free-living  
32 organisms, including SAR11 and *Synechococcus*, appeared on particles, albeit at lower  
33 abundance than in the free-living fraction, suggesting that aggregation processes may  
34 incorporate them into particles. Our approach opens a door to a more quantitative  
35 understanding of the microscale and macroscale biogeography of marine microorganisms.

36 **Abbreviated Summary**

37 We examined bacteria that live on microscopic particles of six different sizes, and not on  
38 particles at the surface and bottom of six locations (some locations lacked oxygen) in the  
39 Chesapeake Bay. Most of the bacteria that live on particles live on the smallest particles,  
40 because those particles are the most abundant. However, some bacterial groups, especially  
41 ones that change the water's sulfur and nitrogen chemistry are often most abundant on particles  
42 of intermediate size.

43

44 **Graphical Abstract**



45  
46

47 **Introduction**

48 Marine environments exhibit microscale heterogeneous environmental conditions and  
 49 bacterial communities vary on the scale of microns to millimeters (Long and Azam 2001; Simon  
 50 et al. 2002; Azam and Malfatti 2007; Stocker 2012). A main contributor to the ocean's  
 51 microscale heterogeneity are particles that vary in size, shape, density, and chemical  
 52 composition (Alldredge and Silver 1988). These particles are habitats for microorganisms whose  
 53 metabolic and behavioral niches differ from those of free-living organisms (Simon et al. 2002;  
 54 Leu et al. 2022). Particle attached bacteria experience environments with more abundant  
 55 energy sources, harbor more diverse genes for breakdown of peptides and carbohydrates, and  
 56 are more densely packed, than are free-living bacteria (Alldredge et al. 1986; Simon et al. 1990;  
 57 Leu et al. 2022).

58 Not only are free-living microbial communities different than particle-attached ones (DeLong  
 59 et al. 1993; Bidle and Fletcher 1995), there is also substantial variability between the microbial  
 60 community on different particles (Mestre et al. 2017; Farnelid et al. 2018). The differences  
 61 between microbial communities on particles of different size (such as on 20 – 200  $\mu\text{m}$  vs 0.8 – 3  
 62  $\mu\text{m}$  particles) are of similar magnitude to those on particles of the same size found at different  
 63 layers of the deep ocean water column (such as the surface and the mesopelagic) or in different  
 64 ocean basins (such as the Pacific and the Atlantic Oceans) (Mestre et al. 2018). These  
 65 microbial community structures reflect chemical differences; particles of different sizes are  
 66 believed to harbor different chemistry with larger particles harboring diffusion gradients of  
 67 oxygen and other oxidants such as nitrate, which allow anoxic microzones to form in low-oxygen

68 water and sulfidic microzones to form in anoxic water (Ploug et al. 1997; Stief et al. 2016;  
69 Bianchi et al. 2018; Fuchsman et al. 2019b; Saunders et al. 2019; Raven et al. 2021).

70 The Chesapeake Bay is the largest estuary in the United States and provides a well-studied  
71 model system characterized by high production and active biogeochemical processes (Turk et  
72 al. 2021). The Bay is characterized by high particle abundance, which transport nutrients and  
73 carbon through the system (Sanford et al. 2001; Malpezzi et al. 2013; Palinkas et al. 2019).  
74 Particles transport organic carbon to the middle of the Bay, where it fuels microbial respiration,  
75 depleting the mid-Bay of oxygen (Wang and Hood 2020) and creating a seasonally (summer)  
76 oxygen-starved environment (Testa et al. 2018). Bacteria in the anoxic Bay are known to  
77 produce greenhouse gases including methane (Gelesh et al. 2016) and nitrous oxide (Ji et al.  
78 2018; Laperriere et al. 2019), as well as hydrogen sulfide (Luther et al. 1988), which is toxic to  
79 marine life (Kang 1997; Boyd 2014). Sulfur oxidizing bacteria, responsible for the removal of  
80 hydrogen sulfide and other reduced sulfur species have been identified in the hypoxic Bay  
81 (Crump et al. 2007; Findlay et al. 2015), potentially using nitrogen species as terminal electron  
82 acceptors (Arora-Williams et al. 2022). Methane appears to be produced in the sediments, but  
83 is oxidized in the water column (Reeburgh 1969; Hagen and Vogt 1999; Gelesh et al. 2016).  
84 However, it is unknown whether and on what sizes of particles methane and sulfur cycling  
85 bacteria associate. Bay microbial communities vary across space and season, following the  
86 changes in oxygen/sulfide concentrations (Kan et al. 2006, 2007; Wang et al. 2020; Arora-  
87 Williams et al. 2022). However, no investigation of the spatial variability of particle associated  
88 bacterial communities using modern techniques has been done in the Bay.

89 Highly size resolved measurements from global sampling efforts have shown that particle  
90 size variability promotes microbial diversity globally (Mestre et al. 2018). Previous analyses of  
91 bacterial communities along the particle size spectrum have been semi-quantitative, providing  
92 relative abundance estimates (fraction of the total community), rather than estimates of  
93 quantitative abundance (cells per liter of water or milligram of particle). Therefore, we  
94 implemented a novel size fractionation approach, with seven size fractions, to allow collection of  
95 DNA, microscopic samples, and concentrations of the particles themselves in each size fraction.  
96 We furthermore utilized DNA standards to quantitatively describe microbial distributions along  
97 the particle size spectrum. Here, we describe particle size resolved measurements of microbial  
98 communities and how they vary across space in the Chesapeake Bay.

## 99 **Methods**

100 Samples were collected at six stations along the length of the mainstem of the Chesapeake  
101 Bay (Figure 1A) at the surface and the bottom of the water column between 2019-July-22 and  
102 July-24. Samples were collected at Chesapeake Bay program stations CB3.1 and CB3.2 at  
103 depths of 3 m (Surface) and 7 m (Bottom); CB3.3 at 3 m (Surface) and 7 m (Oxycline); station  
104 CB4.3C at depths of 3 m (Surface) 6 m (Oxycline) and 19 m (Bottom); Station CB 5.1 at 7 m  
105 (Surface) and 32.5 m (Bottom); and Station 5.5 at 3 m (Surface) and 13 m (Bottom). As stations  
106 were located in 13.3, 12.2, 24.1, 27.1, 34.3 and 17.7 m of water respectively, all samples  
107 labeled “bottom” were taken near the bottom of the water column. Samples were collected on  
108 July 22 from stations CB5.1 and CB5.5, July 23 at stations CB4.3C and CB3.3C and July 24 at  
109 stations CB3.2 and CB3.1. Hydrological conditions were assessed during the time of sampling  
110 by querying Chesapeake Bay Program stations (see supplementary results).

111 Approximately 15 L of water was collected per station using Niskin bottles on a shipboard  
112 CTD rosette. Water was removed from the Niskin bottles by opening the lower stopper in order  
113 to collect even those particles that settled below the sampling valve. We collected POM from six  
114 size classes: 500 µm and larger, 180 – 53 µm, 53 – 20 µm; 20 – 5 µm and 5 – 1.2 µm. We  
115 collected DNA from all of the above size fractions and a 1.2 – 0.2 µm size fraction. Sample  
116 processing happened in two phases. In the first phase, particles were size fractioned using  
117 nylon mesh and re-suspended into a particle slurry of particulate matter made of particles from  
118 500, 180, 53, 20, 5 µm size classes. Additionally, during this stage, water containing only  
119 particles smaller than 5 µm and free-living bacteria was saved. In the second phase, particle  
120 slurry from each size larger than 5 µm was collected on filters for analysis of particulate matter  
121 content (GF/C) and molecular analysis (Supore), and for microscopy (formalin preserved water).  
122 Additionally, during the second stage, water that had passed through the 5 µm filter was split,  
123 with half passed through 1.2 and 0.2 µm Supore filters in series for collection of DNA and a 1.2  
124 µm GF/C filter for collection of POM. Additionally, a portion of this water was also preserved for  
125 microscopy analysis. A full description of these two phases can be found in the supplement  
126 (Supplemental Methods; Particle Processing).

### 127 Particulate Organic Matter Mass

128 To measure particulate organic matter mass, GF/C filters were post-weighed and the pre-  
129 and post-weights were compared, as described and reported in Dougherty et al. (2021). Total  
130 organic matter mass per sample was normalized to the volume of water filtered through the  
131 nylon filter and the fraction of rinse water that passed through the GF/C filter. Total particulate  
132 matter mass was calculated following Eqn. 1.

133

$$134 \frac{\text{Particle mass(mg/L)} = \text{Filter Post Weight(mg)} - \text{Filter Pre Weight(mg)}}{\text{Volume Filtered(L)}} * \frac{\text{Total Volume of Rinse Water(L)}}{\text{Volume Rinse Water Used for POM Measurement(L)}} \text{ Eqn. 1}$$

### 135 Isotopic Analysis

136 After mass was measured, GF/C filters were wafted with hydrochloric acid vapor for 24  
137 hours to remove carbonates, dried, packed in both silver and tin capsules, and sent to  
138 University of California Davis Stable Isotope Facility. Blank combusted GF/C filters were also  
139 included in the analysis. Samples were processed for mass spectrometry following their Difficult  
140 Combustion of Solid Samples Protocol (Supplemental Methods; Isotopic Analysis). Total  
141 particulate nitrogen and particulate carbon concentrations were converted into concentrations  
142 by modifying Eqn. 1, substituting the filter mass difference with observed carbon and nitrogen  
143 concentrations.

### 144 Hydrogen Sulfide Measurements

145 Samples for hydrogen sulfide concentration analysis were treated with zinc acetate to stabilize  
146 sulfide and stop biological activity. Hydrogen sulfide concentrations were measured at stations  
147 CB3.3C and CB4.3C using a colorimetric assay, separately at Horn Point Laboratory (Station  
148 CB4.3C) and at Johns Hopkins University (all depths at station CB3.3C and 21.9m at CB4.3C)  
149 (Cline 1969; Parsons 1984).

150 Measuring Microbial Diversity and Abundance

151 Microbial abundance on selected samples was measured from the formalin preserved  
152 particles by removing the bacteria from the particles by adding detergent and sonicating, and  
153 then enumerating bacteria using DAPI based autofluorescence microscopy (Supplemental  
154 Methods: Microscopy measurements of bacterial abundance). DNA was extracted from the  
155 Supore filters using an in-house phenol chloroform process (modifying Fuhrman et al. 1988;  
156 Cram et al. 2016) (Supplemental Methods; DNA Extraction). Prior to amplification, 10<sup>5</sup> copies of  
157 a synthetic 16S rRNA sequence that has an identity distinct from any known organism  
158 (GenBankAccession Number LC120931; Turlousse et al. 2017) was added per ng of  
159 environmental DNA. DNA was amplified with slight modifications to Needham et al.'s published  
160 protocol (2018) (Supplemental Methods; Amplicon Libraries). Amplicon sequence variants were  
161 called using the DADA2 algorithm (Callahan et al. 2016), following a modified version of Lee et  
162 al.'s (2019) protocol (Supplemental Methods; Amplicon Bioinformatics).

163 Taxon Specific Abundance Estimation

164 To estimate the environmental abundance of each ASV, each ASV sequence read count  
165 was normalized to spike in read counts, the total amount of DNA extracted from each sample,  
166 volume of water filtered, and rinse water volume following Eqn. 2.

167 
$$\frac{\text{Taxon Abundance}(16S + 18S \text{ copies}/L) = \frac{\text{ASV Reads} \cdot 10^5 \text{ Spike Copies} \cdot \text{DNA Extracted}(ng)}{\text{Spike Reads} \cdot 1ngDNA} \cdot \frac{\text{Total Volume of Rinse Water}(L)}{\text{Volume Filtered}(L) \cdot \text{Volume Rinse Water Used for DNA Extraction}(L)} \text{ Eqn 2.}$$

168 Taxon abundance was further normalized to the width of the particle size fraction bins (Eqn  
169 3.)

170 
$$\text{NormalizedTaxonAbundance}(\text{copies}/L/\mu\text{m}) = \frac{\text{Taxon Abundance}(\text{copies}/L)}{\text{SizeClassUpperBound}(\mu\text{m}) - \text{SizeClassLowerBound}(\mu\text{m})}$$
  
171 Eqn 3.

172 To estimate microbial cells per mg of particle mass, microbial abundance was normalized to  
173 particle mass (Eqn. 4).

174 
$$\text{Taxon Abundance}(\text{copies}/\text{mg}) = \frac{\text{Abundance}(\text{copies}/L)}{\text{Particle mass}(\text{mg}/L)} \text{ Eqn. 4.}$$

175 Analytical approach

176 Alpha diversity

177 We used the `breakaway` package (Willis et al. 2018) to estimate species richness in each  
178 of our samples and used the `beta` function therein to explore how richness varied with latitude,  
179 depth and particle size. We used a polynomial model, in which we included a squared term for  
180 latitude and particle size to identify whether richness was highest or lowest at intermediate  
181 salinities and particle sizes.

182 We calculated the Shannon index (H) of diversity using the `vegan` package, first rarefying  
183 samples to 806 reads, which was the lowest number of reads in any of the samples that were  
184 included in the analysis. We estimated Pielou's evenness index (J), by dividing the Shannon  
185 index (H) by breakaway's estimate of evenness (ignoring breakaway's confidence intervals). We  
186 applied ordinary least squares linear models, using R's base `stats` package to estimate the

187 relationship between the Shannon diversity and Pielou evenness scores and particle size,  
188 salinity and oxygen, again including polynomial terms for salinity and depth. For consistency we  
189 also used the linear model to estimate how the richness estimates (from `breakaway`) varied  
190 with size, latitude and depth. Thus between the `beta` function (Willis et al. 2018) and the linear  
191 model, we had two different models of how richness varied with size, salinity and oxygen.

## 192 *Beta Diversity*

193 Overall community patterns and their relationship to sample latitude, depth and size were  
194 summarized by using the `rda()` function in the `vegan` package (Oksanen et al. 2013) on log-  
195 transformed volume and bin size normalized microbial abundance values (cells/L/ $\mu\text{m}$ ).  
196 Significance testing was performed using a permutation test for redundancy analysis as  
197 implemented in vegan's `anova.cca()` function. To reduce computational complexity and  
198 challenges from zero inflation, we only included ASVs in the analysis that appeared in at least  
199 20% of samples.

## 200 *Community structure*

201 Abundance of microbial taxa, grouped to different taxonomic levels were visualized and  
202 representative examples shown herein. We estimated Phylum level abundance patterns by  
203 summing the abundance of all ASVs within each phylum and then reporting only those phyla  
204 that comprised at least  $10^6$  copies/mg particles total, in any of the samples from the 1.2  $\mu\text{m}$  or  
205 larger samples. To explore patterns within one phylum, we visualized all ASVs within the  
206 Planctomycetes phylum considering only ASVs that comprised at least  $10^6$  copies/mg of  
207 particles in the particle containing samples. Planctomycetes were chosen as the representative  
208 phyla for three reasons: (1) they are known to be a major clade of bacteria that are  
209 predominately particle associated (DeLong et al. 1993; Fuchsman et al. 2012), (2) they are  
210 abundant and widespread in the Bay (Kan et al. 2006), and (3) they are important players in the  
211 marine carbon and nitrogen cycles (Shu 2011). We also visualized the abundance of those  
212 bacteria that were most abundant on particles 20  $\mu\text{m}$  or larger. In this case we only showed  
213 ASVs that had an abundance of at least  $10^3$  copies/mg particles on any one sample.

## 214 *Estimating biogeochemical function*

215 To identify bacteria involved in sulfur cycling and methanotrophy, we used tools from  
216 `PICRUSt2` (Douglas et al. 2020) to identify which ASVs had most closely sequenced relatives  
217 that harbored genes for methanotrophy (particulate monoxygenase; EC:1.14.18.3) and for  
218 sulfur cycling (dissimilatory sulfite reductase; EC:1.8.99.5) from the Kegg EC enzyme database  
219 (Kanehisa 2017). From within the `PICRUSt2` package, we aligned the sequences with a  
220 reference tree using `HMMER`, found the most likely placements of each ASV on that reference  
221 tree with `EPA-NG` (Barbera et al. 2019) and output a tree file with `GAPPA` (Czech et al.  
222 2020), using `PICRUSt2`'s `place\_seqs.py` command. We then used the `hsp.py` function that  
223 implements the `castor` algorithm (Louca and Doebeli 2018) to predict gene families associated  
224 with each ASV. While the pipeline for `PICRUSt2` conventionally extends to predicting  
225 metagenomic potential of the overall community, we stopped after gene prediction, and instead  
226 identified which ASVs were associated with our two genes of interest.

227 To identify bacteria putatively involved in nitrogen cycling, we identified ASVs with in which  
228 any taxonomic identifier, from class to genus level, began with the string "Nitro-", and confirmed

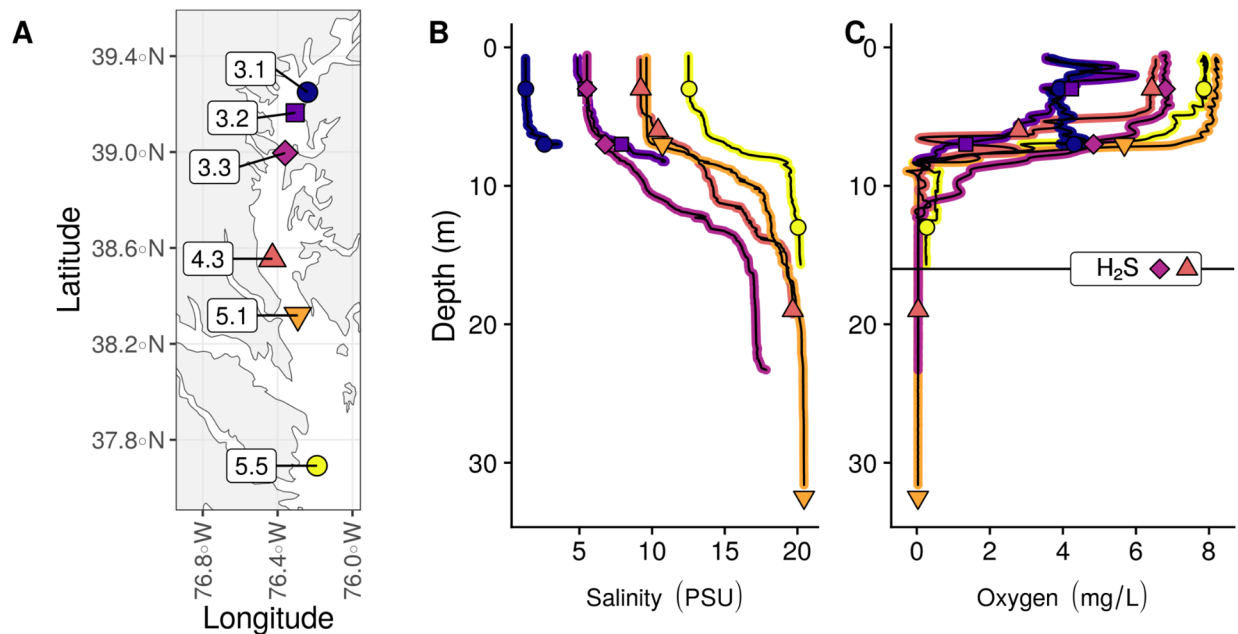
229 that these were known ammonium and nitrite oxidizing organisms. Similarly to identify bacteria  
230 involved in methanotrophy, we searched for archaea with taxonomic identifiers beginning with the  
231 string “Methano-” (Garcia et al. 2000) and for archaea from the Verstraetearchaeota phylum  
232 (Vanwonterghem et al. 2016). We visualized the abundance of these particularly  
233 biogeochemically interesting ASVs, including only ASVs that have an abundance of at least 10<sup>5</sup>  
234 copies/L in at least one size fraction.

## 235 Results

### 236 Site description

237 As reported previously (Dougherty et al. 2021), stations follow a salinity gradient with  
238 northernmost stations less saline than more southerly stations. All sites are characterized by a  
239 pycnocline between 5 and 10 m in depth, with a sharp oxycline at the central Bay stations  
240 CB3.3 and CB4.3C (Figure 1A-C). There was an observed gradient of hydrogen sulfide at  
241 stations CB3.3C and CB4.3C, which was evident from a sulfide smell in the water. A detailed  
242 profile of hydrogen sulfide was measured at CB3.3C and CB4.3C with a notable increase below  
243 15 m at both stations (Figures 1C, S3). Hydrography corresponding to our times of sampling are  
244 described in supplement.

245



246

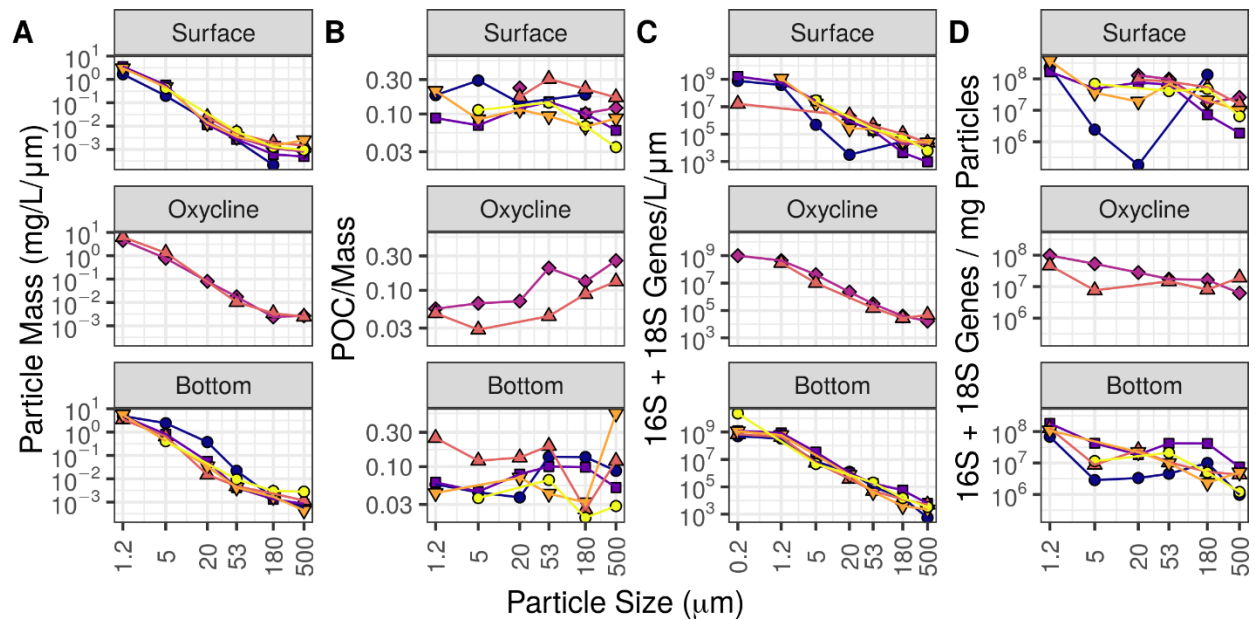
247 Figure 1. Description of the physics and chemistry of the sample sites **A**. Map of all sample sites  
248 – color and shape coding of sites corresponds to point color and shape in panels B and C.  
249 Stations correspond to the Chesapeake Bay Program sampling grid, all station names begin  
250 with the prefix “CB,” and stations 3.3 and 4.3 correspond to central Bay stations and end with  
251 the suffix “C”. For instance, “4.3” corresponds to station “CB4.3C.” **B**. Vertical profiles of Salinity  
252 and **C**. Oxygen. The horizontal line in C, labeled with H<sub>2</sub>S, indicates the depth at which  
253 hydrogen sulfide exceeds 16 μM at station CB3.3C and where the water is also sulfidic at  
254 CB4.3C (Figure S3). In B and C shape position of each point along the depth axis shows the  
255 depth of microbial sampling.

256 Particle composition

257 As reported previously, particle mass follows an inverse power law relationship with particle  
258 size (Dougherty et al. 2021) (Figure 2A). Particle carbon and nitrogen mass both also follow  
259 power laws with respect to size (Figure S4A-C). Generally, carbon comprises ~3 – 30% and  
260 nitrogen ~0.3 – 3% of total particle mass, regardless of particle size (Figure S5AB). Carbon to  
261 nitrogen ratios vary between environments, with highest relative nitrogen content at the  
262 northernmost stations CB3.1 (C:N, integrated over all size classes Surface = 9.6, Bottom = 9.2)  
263 and CB 3.2 (C:N Surface = 8.6, Bottom = 7.8), and highest relative carbon content at station  
264 CB4.3C (C:N Surface 24.3, Oxycline = 16.0, Bottom = 29.0) but are consistently well above the  
265 Redfield ratio (C:N = 6.6; Figure S5C), indicating degraded material.  $\delta^{13}\text{C}$  appears to vary  
266 latitudinally at the surface, running between -23 and -30‰ with least negative values at the  
267 southernmost stations, and most negative values at the terrestrial stations (Figure S6A), as  
268 would be expected due to the isotopic composition of terrestrial (more depleted) and marine  
269 (less depleted) organic matter (Arthur et al. 1985). In bottom waters, the least negative values  
270 appear to be found at the intermediate stations, though these patterns vary between size  
271 classes.  $\delta^{15}\text{N}$  values appear to usually be around 10‰ with some specific samples having  
272 higher values (Figure S6B).

273 Microbial Total Abundance

274 Amplicon sequences suggested acceptable sequence quality data, as evidenced by sequencing  
275 of mock communities (Supplemental Results). Microbial 16S and 18S gene abundances,  
276 generated by this approach, ranged in abundance between size fractions with around  $\sim 10^9$   
277 copies per L of free living bacteria, and fewer bacteria associated with progressively larger size  
278 fractions (Figure 2C). This decrease in microbial abundance tracked the decrease in particle  
279 abundance with their generally being of  $10^7$  -  $10^8$  copies per mg of particle mass, regardless of  
280 particle size or location (Figure 2D). The exception was samples taken at the northernmost,  
281 least saline station CB3.1. There, microbial abundance on intermediate sized particles (5 – 53  
282  $\mu\text{m}$ ) was between  $10^5$  –  $10^6$  copies per mg. We expect these abundances are likely slight (same  
283 order of magnitude) over-estimates of total microbial abundances because single cells often  
284 harbor multiple 16S or 18S gene copies (Větrovský and Baldrian 2013). Consistent with this,  
285 amplicon-based estimates of microbial abundance were generally within the same order of  
286 magnitude as, though slightly higher than, microscopy-based estimates (Figure S8), as  
287 expected from organisms that harbor multiple 16S and 18S gene copies per cell.



288  
 289 Figure 2. Free living and particle associated microbial total abundance at each station and  
 290 depth. **A.** Total particle mass, normalized to particle size bin width. **B.** The ratio of particulate  
 291 carbon mass to total particle mass. **C.** Microbial abundance per liter of water, normalized to  
 292 particle size bin width. **D.** Microbial abundance normalized to particle mass. In all panels, both X  
 293 and Y axes are on a log scale. Line and symbol colors indicate stations as seen in Figure 1.

294 Alpha diversity

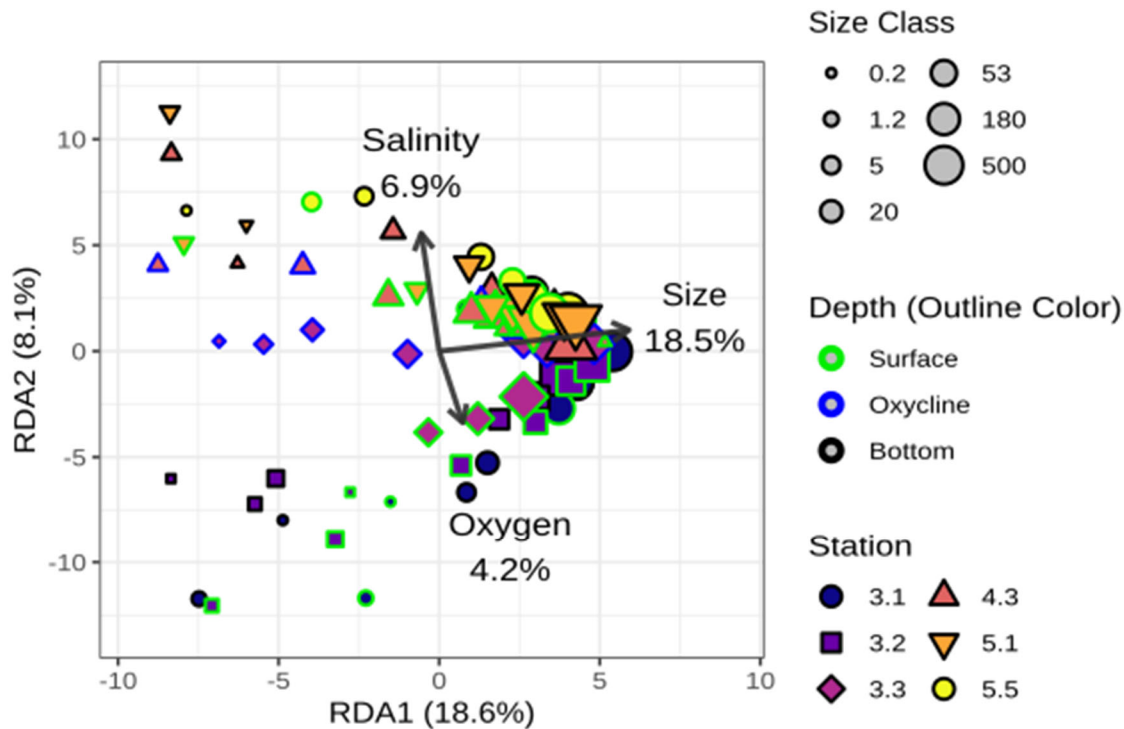
295 Across our entire dataset, we observed 82476 unique ASVs, excluding ASVs that mapped  
 296 to our spike-in samples. The breakaway package, which estimates the abundance of  
 297 unobserved singleton species, estimated that sample richness ranged from 23 (lower bound  
 298 22.1, upper bound 39.3) to  $10.2 \times 10^3$  (bounds:  $4.90 \times 10^4 - 2.77 \times 10^5$ ) ASVs per sample (Figure  
 299 S9A). The `betta` function, which accounts for the abundance of these unobserved species on  
 300 richness patterns (Willis et al. 2018) showed non-linear relationships with particle size and  
 301 salinity ( $p < 0.001$ ; Figure S10A; Table S4), with highest richness among intermediate sized  
 302 particles (5–20  $\mu\text{m}$  and 20–53  $\mu\text{m}$  size bins; Figure S10A). Richness appeared to be unrelated  
 303 to dissolved oxygen concentration (Table S4;  $p = 0.779$ ). Applying a simpler linear model, rather  
 304 than the `betta` function showed similar but weaker patterns (Table S4). Thus, for our data, the  
 305 `betta` algorithm is consistent with, though more sensitive than, the linear model.

306 Linear models further suggested that the Shannon diversity index (Figures S9B, S10B) was,  
 307 like richness, highest among intermediate particle sizes (5 – 20  $\mu\text{m}$ , 20 – 53  $\mu\text{m}$ , and 53 – 180  
 308  $\mu\text{m}$  size bins; Table S4). Evenness (Figures S9C, S10C) was non-statistically significantly  
 309 lowest among intermediate sized particles ( $p = 0.053$ ) and did not vary with any other  
 310 parameters (Table S2).

311 Beta Diversity

312 Redundancy analysis suggested that overall microbial community structure (normalized to  
 313 volume filtered and bin-size, and expressed as copies/L/ $\mu\text{m}$ ) was statistically related to particle

314 size, water salinity and water oxygen concentrations (Figure 3; Figure S11; Table S3; ANOVA  $p$   
315  $< 0.01$  for all terms).



316  
317 Figure 3. Redundancy analysis of the relationship between community structure and salinity,  
318 oxygen concentration and particle size. Both size and oxygen data have been log transformed.  
319 Axes correspond to the first two redundancy analysis axes and show 18.6% and 8.1% of the  
320 variance. Points indicate samples and their outline colors, fill colors and shapes (corresponding  
321 to stations indicated in Figure 1A) and sizes indicate which station, depth and size class they  
322 were collected from (legend). Arrows indicate the three terms in the RDA model: particle size,  
323 salinity, and dissolved oxygen concentrations. Percentages by each arrow show the marginal  
324 percentage of variance explained by that parameter.

325  
326 Similar patterns were evident when samples from the 0.2 – 1.2  $\mu\text{m}$  fraction were removed,  
327 and when samples from the 0.2 – 1.2 and 1.2 – 5  $\mu\text{m}$  fractions were both removed (Figure S12;  
328 Table S5), indicating that community structure differs across the particle size gradient and is not  
329 driven only by differences between free-living and attached bacteria. Similar patterns were also  
330 observed, when latitude, depth (whether the sample was collected from near the surface) and  
331 size (hereafter Positional Model) were compared to community structure (Figure S13A,B), rather  
332 than salinity, oxygen and size (hereafter Environmental Model). In both cases, the predictor  
333 variables explained a similar fraction of total variance (Environmental Model 26.3%; Positional  
334 Model, 25.4%). We found that adding sample depth to the Environmental Model did not result in

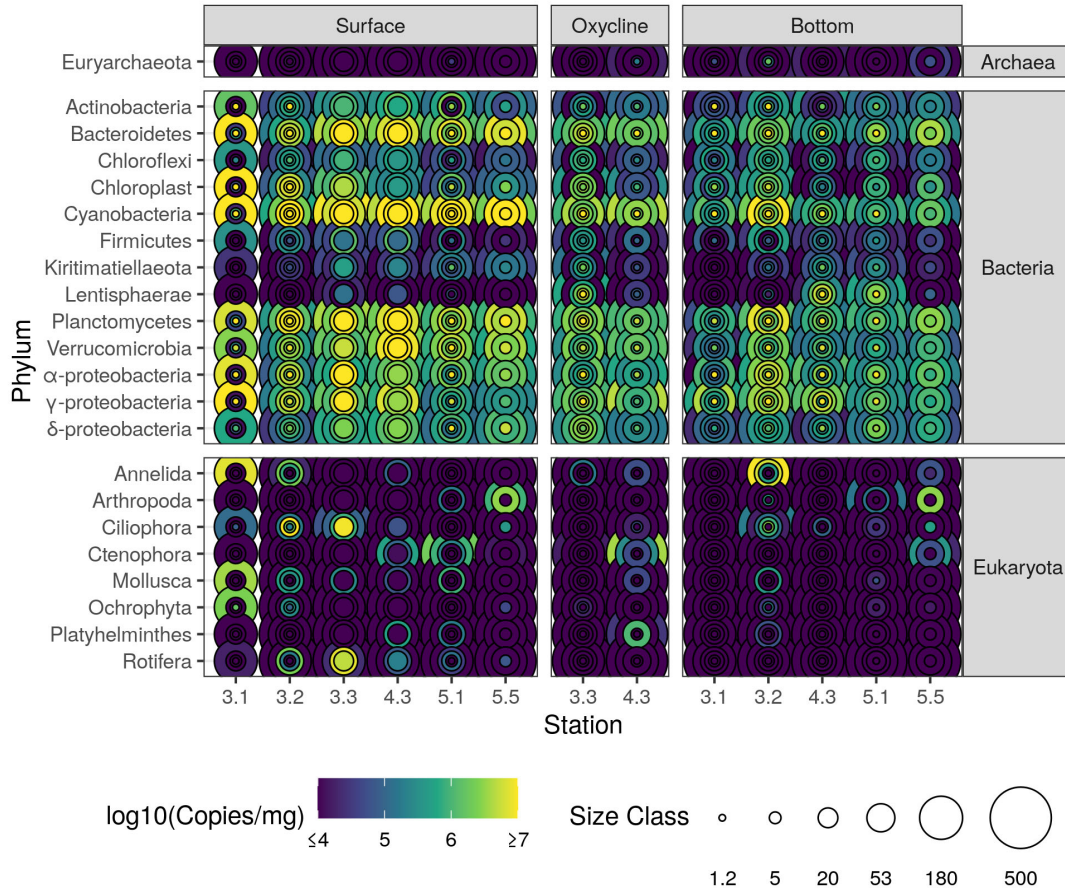
335 an increase in model performance (ANOVA;  $p = 0.31$ ). For both models, adding quadratic terms  
336 lead to an increase in model performance, with lower AIC values (Environmental Model, DF = 4,  
337 AIC = 681; Quadratic Environmental Model, DF = 6, AIC = 677; Positional Model, DF = 4, AIC =  
338 682; Quadratic Positional Model, DF = 6, AIC = 677) and higher percent variance explained  
339 (Quadratic Environmental, 34.3%; Quadratic Positional, 34.1%). Adding information about  
340 carbon to mass ratio, carbon to nitrogen ratio,  $\delta^{13}\text{C}$  or  $\delta^{15}\text{N}$  values of the particles to the  
341 Environmental Model did not appear to lead to a statistically detectable increase in model  
342 performance. (ANOVA;  $p$  of all new terms  $> 0.05$ ). Indeed, a stepwise regression in which non-  
343 significant terms were dropped from the model in order of lowest significance found that each of  
344 these new terms was eliminated from the model.

#### 345 Diversity Patterns

##### 346 *Phylum Level*

347 It was clear that some microbial taxa were associated in particular with some stations,  
348 depths and particle size fractions. Normalized to particle mass, bacteria from the phyla  
349 Bacteroidetes, Cyanobacteria, Planctomycetes, Verrucomicrobia and Alpha-, Delta- and  
350 Gamma- Proteobacteria were all abundant on particles, each with higher abundance at the  
351 surface of all stations, the bottom of station CB3.2, and the oxycline of station CB3.3C (Figure  
352 4). Archaea in contrast were rarely abundant on particles. Euryarchaeota were abundant on  
353 small particles at station CB3.2 Bottom and CB4.3C Oxycline. Diverse eukaryotes, especially  
354 meso-zooplankton and Ochrophyta (diatoms and other brown algae) were detected and  
355 abundant at least at some stations. All were associated primarily with intermediate and large  
356 size classes, likely reflecting the larger size of these organisms.

357 Normalized to water volume, rather than particle mass, all particle associated phyla were  
358 primarily associated with the smallest particles (Figure S14). This is because even if the  
359 microorganisms are abundant relative to particle mass, most particle mass is associated with  
360 small particles (Figure 2A-B).



361

362 Figure 4. Phylum level taxonomic groups, measured as 16S or 18S rRNA gene sequences  
 363 per mg of particulate mass, in all three domains of life. Phyla are in rows, with kingdoms shown  
 364 in the panels at right. Stations are in columns with panels at top showing sample depth  
 365 (Surface, Oxycline, Bottom); latitude for each station is shown in Figure 1A. Concentric circles  
 366 indicate each size class of particles. Color corresponds to log transformed abundance of each  
 367 microbial group. Some size classes at some stations are not shown, because either particle  
 368 mass or amplicon measurements were not successful. Only phyla whose abundance exceeds  
 369  $10^6$  cells/mg particles, in at least one sample, are shown. The Proteobacteria phylum was  
 370 subdivided into class, and Chloroplasts, while technically Cyanobacteria under the SILVA  
 371 taxonomic scheme, are treated as their own phylum.

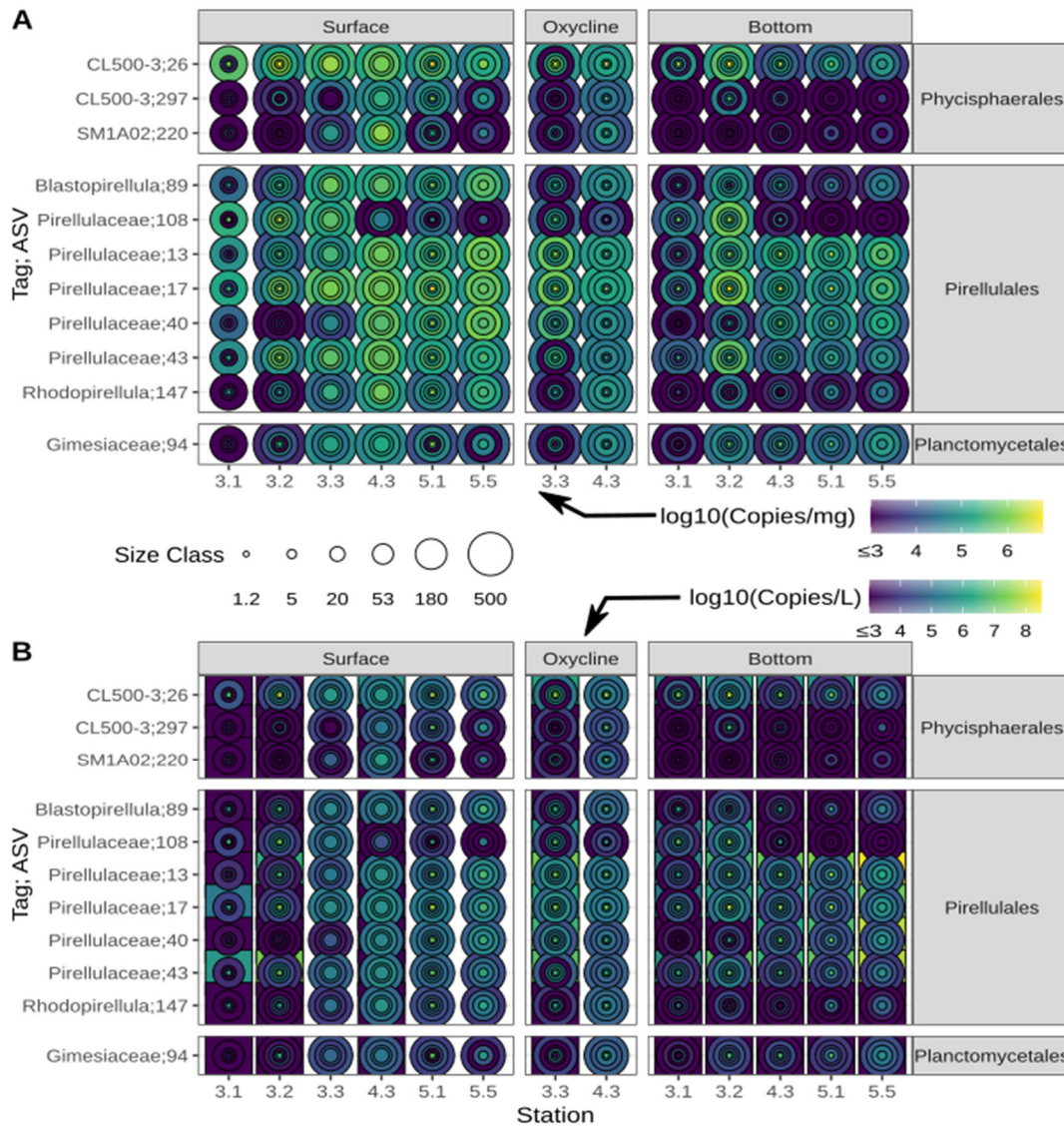
372

373 *ASV Level*

374 As with the phyla level patterns, some ASVs were abundant when normalized to particle  
 375 mass, but were scarce when normalized to water volume. This pattern occurs because large  
 376 particles are scarce relative to small ones (Dougherty et al. 2021) and so comprise less habitat.  
 377 An example of this pattern is the ASV level groups of Planctomycetes, which fall into three  
 378 families (Phycispareles, Pirellulales and Planctomycetales). ASVs showed associations  
 379 especially with high or low latitude stations, and some with surface or bottom waters. Some  
 380 were primarily associated with small particles, and others with all sizes of particles (Figure 5A).

381 However, normalized to water volume, all Planctomycetes ASVs were primarily associated with  
 382 the free-living and 1.2 – 5  $\mu\text{m}$  size fractions (Figure 5B).

383



384

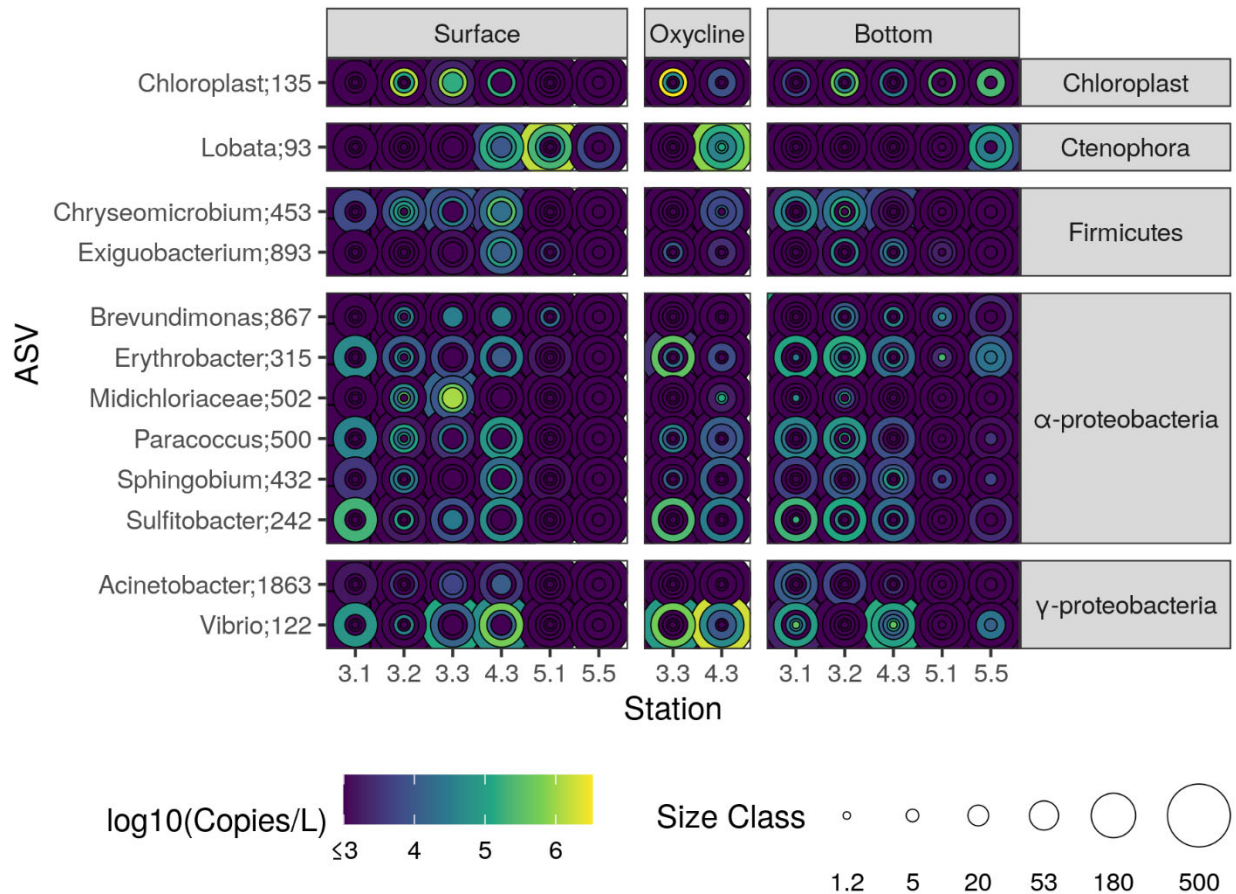
385

386 Figure 5. Abundance of different amplicon sequence variants from within the phylum  
 387 Planctomycetes. ASVs are rows, with order level taxonomy on the panels at right. Depths and  
 388 stations are indicated by column, as in Figure 4. **A.** Normalized to particle mass. **B.** Normalized  
 389 to volume of water. Axes as in Figure 4. Only ASVs whose abundance exceeds  $10^6$  cells/mg of  
 390 particles, in at least one sample, and that appear in at least 20% of all samples, are shown. ASV  
 391 number is indicated after a semicolon.

392

393 A few ASVs showed an exception to the pattern in which most were associated with small  
 394 particles. Six ASVs from the Alphaproteobacteria class and two each from the

395 Gammaroteobacteria class and Firmicutes phylum were primarily associated with size classes  
 396 20  $\mu\text{m}$  or larger (Figure 6), were at least  $10^6$  cells/ml in one sample, and were observed in at  
 397 least 20% of all samples. These species included known parasites such as an ASV from the  
 398 Midichloraceae family, as well as others known to break down particulate matter such as one  
 399 ASV from the Paracoccus genus, which BLAST against the NCBI database indicated was  
 400 identical to two species: *Marcusii* and *P. Carotiniaciens*. Also evident in the larger size fractions  
 401 were larger organisms. These included an ASV from the Lobata order (ctenophore) and a  
 402 chloroplast for which NCBI Blast search reported 100 percent similarity to several eukaryotic  
 403 algae, including both diatoms and foraminifera.



404  
 405 Figure 6. Abundance of different bacterial amplicon sequence variants that are most  
 406 abundant, on average, on size fractions 20  $\mu\text{m}$  or larger, normalized to volume of water. Axes  
 407 as in Figure 4. Only ASVs whose abundance exceeds  $10^4$  cells/mg of particles, in at least one  
 408 sample, and that appear in at least 20% of all samples, are shown. ASV number is indicated  
 409 after a semicolon.

410  
 411 All bacterial ASVs that were abundant ( $\geq 1\%$  of the total community) in the 0.2 – 1.2  $\mu\text{m}$ ,  
 412 free-living size fraction were also found at lower, but still detectable abundance, in larger size  
 413 fractions (Figure S15A-C). These included several bacterial ASVs from the SAR11 clade, which  
 414 is ostensibly free living.

415 Bacterial influences on biochemical cycling

416 A range of bacteria potentially involved in methane, sulfur and nitrogen cycling, were  
417 identified by observing taxonomic identities, in the case of methanogenic and nitrogen cycling  
418 organisms; and using PICRUSt2 to identify bacteria with closest known relatives with that  
419 harbored the gene for dissimilatory sulfite reduction enzyme, in the case of sulfur cyclers; and  
420 the particulate monooxygenase enzyme in the case of methanotrophs (Figure 7). All of these  
421 biogeochemical processes were dominant in the bottom or oxycline samples, when they were  
422 observed.

423 Methane cycling

424 Methanotrophy: The PICRUSt2 based approach identified one species whose closest fully  
425 sequenced relative harbored the particulate monooxygenase enzyme EC:1.14.18.3, which is  
426 involved in methanotrophy with oxygen. This was an otherwise unidentified ASV from the  
427 Methylomonaceae family. This putative methanotroph was abundant particularly in the smallest  
428 particle size fraction (1.2 – 5 µm) in the bottom waters of all but two stations (Figure 7). At  
429 station 3.2 it was abundant on 20 – 53 µm and 53 – 180 µm particles, rather than the smallest  
430 size fraction. It was not abundant in any size fraction at the southernmost station CB5.5.

431 Methanogenesis: We identified one ASV that was potentially methanogenic, an unidentified  
432 ASV from the Methanofastidiosales order. This ASV was only found in one sample, the free-  
433 living (0.2 – 1.2 µm) size fraction at the bottom depth of station CB5.1 at an abundance of  $1.6 \times$   
434  $10^5$  16S gene copies/L seawater. No other groups were identified in our dataset with the prefix  
435 of Methano- in any of their taxonomic identifications from Class through Genus level (Garcia et  
436 al. 2000), nor were any bacteria from the Verstraetearchaeota phylum (Vanwonterghem et al.  
437 2016) identified. This absence suggests that no other methanogens were present in our dataset.

438 Nitrogen Cycling

439 Ammonium oxidizing and nitrite oxidizing taxa were both evident at our site and were  
440 primarily found in bottom waters. Ammonium oxidizing archaea from the genus *Candidatus*  
441 *Nitrosopumilus* were found free-living in all stations except for the northernmost CB3.1 and most  
442 ASVs were also associated with the smallest particle size fraction at most of these sites.  
443 Ammonium oxidizing bacteria, one each from the genera *Nitrosoglobus* and *Nitrosomonas*  
444 genera were seen, with the *Nitrosomonas* found at the northernmost stations CB3.1 and CB3.2,  
445 again primarily free-living and on the smallest particle size fraction. *Nitrosoglobus* was found  
446 only in the free-living fraction at station CB5.5 and in no other samples. Nitrite oxidizing bacteria,  
447 all of the genus *Nitrospira*, showed a different pattern, in which they were primarily associated  
448 with intermediate sized particles (5 – 20 µm and 20 – 53 µm) at stations CB3.1 and CB3.2,  
449 though one ASV was abundant on particles at station CB3.2.

450 Sulfur Cycling

451 Multiple and diverse Proteobacterial species harbored the dissimilatory sulfite reduction  
452 enzyme EC:1.8.99.5. These included many putative sulfate-reducing Deltaproteobacteria,  
453 several sulfur oxidizing bacteria from the family Sedimenticolaceae, a purple sulfur bacteria  
454 ASV, and a purple nonsulfur bacteria ASV.

455 The sulfate-reducing Deltaproteobacteria fell into four families, with biogeographical patterns  
456 more or less conserved within the families. Desulfarculaceae were primarily associated with the  
457 smallest size class of particles, though also found on larger particles at all stations south of and  
458 including CB3.3C. Desulfobacteraceae had a similar pattern but were sparse at the  
459 southernmost station CB5.5. Most members of this phyla were also present on the largest  
460 particle size fraction at station CB3.3 and intermediate size fraction at station CB4.3.  
461 Desulfovibrionaceae appeared to be both free-living and associated with the smallest size  
462 fraction (1.2 – 5 µm), though at station 3.3 some were also associated with the largest ≥ 500 µm  
463 size class. Desulfobulbaceae at station CB3.3 was most abundant in intermediate size fractions  
464 (20 – 53 µm and 53 – 180 µm). A single ASV (Desulfofustis; 617) was also found on  
465 intermediate sized particles at the northernmost stations CB3.1 and CB3.2. At stations CB4.3C  
466 and CB5.1, this Desulfobacteraceae was predominantly found on smaller particles. Thus  
467 Desulfobulbaceae tended to associate with different particle sizes depending on salinity. Some  
468 Desulfobulbaceae can reverse their sulfur reduction pathway (Trojan et al. 2016), and so may  
469 oxidize sulfur.

470 Sulfur oxidizing bacteria included both photosynthetic (purple sulfur and non-sulfur bacteria  
471 Bryant and Frigaard 2006) and non-photosynthetic (Sedimenticolaceae) members. Sulfur  
472 oxidizing bacteria from the Sedimenticolaceae family appeared to largely co-occur with sulfate  
473 reducing bacteria. They were found both free-living and in all size classes, though which size  
474 classes they were found in varied between stations. One ASV of purple sulfur bacteria, which  
475 was identified to the Chromatiales order appeared primarily in the smallest size class at the  
476 most anoxic stations (CB3.3C, CB4.3C and CB5.1), though it also showed up in larger particles  
477 at stations CB3.2 and CB3.3C. Similarly, one ASV of purple nonsulfur bacteria, identified to the  
478 Rhodospirillaceae family, was found at all Station CB3.3C and south, and was primarily free-  
479 living, though at stations CB4.3C and CB5.1 was also associated with the smallest particle size  
480 class.



500 Figure 7. Abundance of bacterial ASVs that are putatively involved in methanogenesis,  
501 methanotrophy, nitrogen cycling or sulfur cycling (see methods for how functionality was  
502 determined). Panels are grouped vertically by biogeochemical *process* type, Class and Family.  
503 Parentheses indicate biogeochemical processes in which all members of a given clade are  
504 involved, and whether a given Class is from the Archaeal domain. ASV number is indicated after  
505 a semicolon.

## 506 **Discussion**

507 While our approach gives consistent results with previous size fractionation based studies  
508 (Mestre et al. 2018), that bacterial communities vary with particle size, location and depth  
509 (Figures 3, S11, S12), the more quantitative approach employed in this project extends these  
510 results by identifying the sizes of particles in which microorganisms primarily reside. We present  
511 six novel observations (I- VI). Specifically, we showed that (I) particle associated microbial  
512 abundance scales linearly with particle mass, (II) most organisms are free-living or associated  
513 with the smallest particle size class, while only a few organisms associated primarily with larger  
514 particles, and (III) there were no abundant free-living bacteria that were not also present on  
515 particles. We also showed that (IV) microbial richness is generally highest on particles of  
516 intermediate size (5 – 180  $\mu\text{m}$ ). Our method allows us to describe (V) the distribution patterns of  
517 the eukaryotic community and size and particle partitioning of some members. Finally, this  
518 approach allowed us to show that (VI) bacteria involved in anoxic processes associated with the  
519 transformation of methane, sulfur and nitrogen were associated primarily with particular particle  
520 sizes in particular regions and depths of the Bay. In this discussion we first explore some  
521 methodological considerations, and then expand on each of these six novel observations.

### 522 Six novel observations

#### 523 (I) Microbial abundance scales linearly with particle mass

524 The observation that bacterial abundance scales with particle mass and particulate organic  
525 carbon mass suggests that bacteria are likely distributed throughout particles, rather than just  
526 on their surface, or that particles are fractal in shape such that their effective surface area  
527 scales linearly with their volume. Such an observation is consistent with prior microscopy based  
528 observations that bacteria are distributed throughout the core of marine particles (Flintrop et al.  
529 2018). The observation that bacterial abundance is lower (by over two orders of magnitude on  
530 the 20 – 53  $\mu\text{m}$  size class than on the same size class at other stations) on particles at the  
531 northernmost station CB3.1 could reflect that these northern particles differ in their physics and  
532 chemistry from those further south in the Bay, such that they support fewer bacteria relative to  
533 their mass. Furthermore, at the bottom of the water column (the only depth this sample was  
534 measured), the CB3.1 site had the fewest ASVs associated with the largest particle size fraction  
535 (breakaway richness estimate of 100 ASVs, vs 1610-2260 ASVs for all 500  $\mu\text{m}$ , bottom water,  
536 samples; Figure S9) and a community structure most distinct from smaller particles (Figure 3),  
537 suggesting a distinct environment at this site. Just north of our northernmost site CB3.1, the Bay  
538 is characterized by an estuarine turbidity maximum (Schubel 1968). This region has high  
539 particle loading and more terrestrial particle origins than elsewhere in the Bay (Schubel 1968;  
540 Sanford et al. 2001; Malpezzi et al. 2013). In particular, the turbidity maximum traps particles of  
541 intermediate sinking speed (Geyer 1993), which could in principle select for particles with

542 elevated mineral ballast content. However, the particles in this region had carbon to mass ratios  
543 and C:N ratios that were similar to those seen elsewhere (Figure 2B), suggesting that relevant  
544 chemical differences, if they exist, extend beyond the carbon to mass ratio. Despite this lower  
545 microbial abundance on particles, estuarine turbidity maximum systems are typified by fast  
546 microbial growth rates (Baross et al. 1994; Lee et al. 2012) especially by particle associated  
547 bacteria (Crump and Baross 2000), and by high particle concentrations (Schubel 1968), and so  
548 particle associated microbial heterotrophic productivity and other biogeochemical process rates  
549 are not necessarily lower at the northernmost site, even though the bacteria are less dense on  
550 particles.

551 (II) Most, but not all, organisms are associated primarily with small particles

552 We showed, for the first time, that most particle associated organisms are primarily  
553 associated with the smallest particles (range 69-99%; Figures 2C, 5, S14). This is true even for  
554 taxa that are more abundant relative to particle mass on larger particles, because small particles  
555 are so much more abundant by number and mass than large ones (Figure 2A). Such a pattern  
556 indicates that the primary habitat of most particle associated bacteria are small particles. As  
557 long as microbial growth rates are not orders of magnitude faster on large particles than small  
558 ones, this pattern would further suggest that most taxa are adapted to small rather than large  
559 particle environments. Small particles are typified by longer residence times than larger particles  
560 (Alldredge and Gotschalk 1988; DeVries et al. 2014), which may select for bacteria able to  
561 capitalize on these more persistent environments (Kiørboe et al. 2003), and higher spherical  
562 surface area to volume ratio allowing for more advection of oxidants throughout the particle  
563 (Weber and Bianchi 2020). However, some taxa are primarily associated with intermediate and  
564 large particles (Figure 6), including methane and sulfur cycling taxa that may favor anoxic  
565 microenvironments (Figure 7).

566 Several ASVs showed exceptions to the above pattern and are primarily associated with  
567 particles 20  $\mu\text{m}$  or larger. Some of these bacteria such as Midochloraceae (Montagna et al.  
568 2013) and Sulfitobacter (Amin et al. 2015; Johansson et al. 2019; Shibl et al. 2020) are known  
569 to be symbionts and may be associated with larger organisms and likely appear in our larger  
570 size fractions because their hosts partition into larger size classes. In contrast, the *Paracoccus*  
571 ASV which was found to associate statistically with large particles likely associates physically  
572 with those particles, rather than large organisms. *Paracoccus* can both grow aerobically and can  
573 break down a variety of sugars and other compounds (Harker et al. 1998; Tsubokura et al.  
574 1999). Thus, it seems probable given their metabolism that the *Paracoccus* ASV is degrading  
575 the large particles. An ASV from the *Vibrio* genus, which we could not classify further with NCBI-  
576 BLAST, was associated especially with the largest size class. Some but not all *Vibrio* are  
577 pathogens (Colwell et al. 1977) and may be associated with zooplankton (Kaneko and Colwell  
578 1973), but many are also known to associate with suspended particles (Froelich et al. 2013;  
579 Kirstein et al. 2016; Liang et al. 2019), and could be in either role in this environment.

580 (III) We observed no exclusively free-living, abundant, bacteria

581 The observation that every ASV that comprised  $\geq 1\%$  of the free-living community was also  
582 found associated with some particle size fraction indicates that all abundant bacteria in the Bay  
583 mainstem are at least sometimes associated with particles, at least at the time and locations

584 where we sampled. This is in contrast to observations of the Baltic Sea, where it was shown that  
585 many bacterial species were only found in the free-living fraction (0.22 – 5  $\mu\text{m}$ ; Rieck et al.  
586 2015). However, SAR11 bacteria which are believed to be free-living in nature (Giovannoni et  
587 al. 2005) and grow free-living in culture (Rappé et al. 2002), are seen not only associated with  
588 particles in our dataset (Figure S15), but also in large size fractions in the more oligotrophic  
589 Blanes Bay microbial observatory in the Mediterranean Sea (Mestre et al. 2020) or in the  
590 Eastern Tropical North and South Pacific (Ganesh et al. 2014; Fuchsman et al. 2017),  
591 suggesting that the association of abundant “free-living” bacteria with particles may happen  
592 elsewhere. One possibility is that free-living bacteria become associated with particles through  
593 physical processes, such as sticking and aggregation, which the bacteria cannot avoid. This has  
594 been shown for *Synechococcus* in the laboratory (Cruz and Neuer 2019). Additionally, viral  
595 infection can cause bacteria to clump (Shibata et al. 1997), and high viral loads on particles of  
596 viruses that infect free-living bacteria support the importance of this pathway (Ganesh et al.  
597 2014; Fuchsman et al. 2019a). As particles are particularly abundant in the tidal Chesapeake  
598 Bay (Dougherty et al. 2021; Turner et al. 2021) perhaps physical aggregation is more  
599 pronounced in the Bay than elsewhere.

#### 600 (IV) Microbial richness is highest on intermediate sized particles

601 The observation that particles of intermediate size (5 – 180  $\mu\text{m}$ ) harbored highest richness,  
602 and thus highest Shannon diversity could indicate that intermediate sized particles have  
603 characteristics of both larger and smaller particles and so harbor communities typical of both  
604 particle types. In other ocean sites, high richness has been seen in transitions between different  
605 communities. For instance, in the oligotrophic coastal ocean richness was high in the  
606 mesopelagic transition between the surface deep ocean environments (Cram et al. 2015). In an  
607 estuary system, richness was shown to be highest in brackish water (Tee et al. 2021).  
608 Meanwhile in sediments, nitrifying bacteria appear to be most diverse at zones of redox  
609 transitions (Zhao et al. 2019).. Perhaps a similar pattern happens along the observed particle  
610 size gradient with intermediate sized particles containing attributes and microorganisms from  
611 both larger and smaller size fractions.

612 The lower diversity in the central Bay opposes patterns seen in the Columbia River and  
613 Waiwera River estuaries, where alpha diversity was higher in brackish waters than elsewhere  
614 (Fortunato et al. 2011; Tee et al. 2021). In our system, the sulfidic waters in the brackish section  
615 of the estuary likely select against many common bacteria. This brackish and sulfidic bottom  
616 environment, because it is smaller than the oceans or watershed systems that surround it, may  
617 be affected by island biogeography effects (MacArthur and Wilson 2001) in which smaller  
618 systems support fewer species.

#### 619 (V) Algal and zooplankton size and spatial distribution patterns

620 In contrast to bacterial phyla, most Eukaryotic phyla appear to have patchy distribution  
621 across space and are often found only associated with particular size classes (Figure 4).  
622 Ochrophyta (diatoms and other brown algae) and Ciliophora (ciliates) are microorganisms that  
623 were abundant in our largest size classes, suggesting that they may aggregate into and/or  
624 associate with particles. (Figure 4).

625 The observation that zooplankton associate with particular size classes reflects the size of  
626 those organisms. For instance, Arthropods, dominated by Maxilopods, were found primarily in  
627 the 53-180  $\mu\text{m}$  size class, suggesting that we have primarily sampled individuals from the  
628 Nauplii or Copepodite life stages. The dominance of sub-adult life stages is consistent with  
629 previous observations (Kimmel et al. 2006), and the fact that adult maxilopods can avoid being  
630 collected in Niskin bottles. Alternatively, these findings could reflect fragments of zooplankton  
631 carapaces and molts being collected on the smaller size filters. The observation that arthropods  
632 are mainly in the Southernmost station, and that they avoid the sulfidic region of the Bay also  
633 reflect previous observations (Zhang et al. 2006). Meanwhile Ctenophora are primarily  
634 associated with our larger size classes reflecting that ctenophores and parts thereof tend to be  
635 larger than 500  $\mu\text{m}$  (Ruppert et al. 2004).

#### 636 (VI) Elemental Cycling

637 Bacteria involved in methane, sulfur and nitrogen cycling were shown to have particle size  
638 and water salinity specific habitats (Figure 7). Putative methane, sulfur and nitrogen cycling  
639 organisms were each most abundant in bottom waters and scarce in surface waters, confirming  
640 that anoxia and/or interaction with the sediment are likely important for all of these processes.  
641 Sulfate reducing and sulfide oxidizing microorganisms have been associated with particles in  
642 other anoxic systems (Fuchsman et al. 2012, 2017; Saunders et al. 2019; Raven et al. 2021),  
643 but their association with particular particle sizes has not been seen before, to our knowledge.

#### 644 *Methane cycle*

645 The observation that methanogens were scarce in our dataset, while methanotrophs were  
646 abundant on particles supports the inference that methanogenesis likely occurs in the sediment  
647 (as shown by Gelesh et al. 2016) and not on suspended particles; but methane is consumed in  
648 the water column primarily by particle associated, rather than free-living, bacteria. Methanotroph  
649 ASVs were present at all stations except station CB5.5 (Figure 7), suggesting that methane is  
650 produced by the sediment across the Bay and consumed in the overlying waters. CB5.5 is more  
651 marine, and this region has lower organic carbon in its sediments (Roden and Tuttle 1993;  
652 Zimmerman and Canuel 2001). Thus, methane is either not produced, or is both produced and  
653 consumed in the sediments.

#### 654 *Nitrogen cycle*

655 Our data suggest that ammonia-oxidizing bacteria and archaea are ubiquitous in the bottom  
656 waters of the Chesapeake Bay, and are primarily associated with the free-living (0.2 – 1.2  $\mu\text{m}$ )  
657 and next-smallest (1.2 – 5  $\mu\text{m}$ ) size fractions. The presence of these organisms in the anoxic  
658 bottom waters of the Bay is surprising, since these nitrifying bacteria and archaea require  
659 oxygen as an oxidant. The ammonia-oxidizing organisms could be either advected or dispersed  
660 into the anoxic bottom waters. However, distinct ammonia-oxidizing archaea have also been  
661 found in the upper sulfidic zone of the Black Sea, implying a more complex lifestyle (Coolen et  
662 al. 2007). Large particles appear not to be important habitats for ammonium oxidizing  
663 organisms. The exception to this pattern was an ASV from the *Nitrosomonas* genus, which  
664 appeared to associate with larger particles in the northernmost stations of the Bay (Figure 7).  
665 *Nitrosomonas* has been found associated with particles previously in the Mediterranean Sea  
666 (Phillips et al. 1999).

667 In contrast, nitrite-oxidizing ASVs from the *Nitrospira* genus appeared to have, as their  
668 primary habitat, particles from the northernmost Bay stations. Such a pattern could suggest  
669 geographic decoupling between ammonium and nitrite oxidation. However, the lack of observed  
670 nitrite oxidizers in the southern station despite the abundance of ammonium oxidizing archaea  
671 suggests that some other unidentified organisms are likely consuming the nitrite produced by  
672 the ammonium oxidizers at these stations.

673 Our PCR primers have mismatches to anammox bacteria (McNichol et al. 2021), and  
674 unsurprisingly we did not detect any anammox bacteria in our dataset. Future efforts should  
675 consider using the pooled primer sets that have since been described by McNichol et al. (2021),  
676 and which better amplify organisms from this group. We did not look for denitrifying bacteria in  
677 our site, as denitrification is not phylogenetically conserved (Zumft 1997; Bertagnolli et al. 2020)  
678 and so neither taxonomic groupings nor phylogenetic placement is likely to generate reliable  
679 information about this process. However this process is common in anoxic systems, and has  
680 been measured in the Chesapeake previously (Ji et al. 2018). Furthermore, new evidence  
681 suggests that many of the taxa associated with sulfur cycling in the Chesapeake also reduce  
682 nitrate (Arora-Williams et al. 2022). Thus, it is likely that many bacteria especially in the anoxic  
683 waters are indeed removing nitrogen from the system.

#### 684 *Sulfur cycle*

685 Sulfur cycling organisms were particularly abundant at the oxycline sample of station  
686 CB3.3C (Figure 7). These sulfur cycling taxa were not as abundant at station CB4.3C's oxycline  
687 depth. Consistent with this, our sulfide profiles indicate that CB3.3 had higher sulfide  
688 concentrations than CB4.3 (Figure S3). These differences could be due to variations in the  
689 benthic sulfide flux (Roden and Tuttle 1992), which can play a role in driving sulfur cycling in  
690 anoxic bottom waters. While sulfide transport out of sediment occurs in the summer at both  
691 sites, site CB3.3C has higher sulfate reduction rates in the winter which may promote higher  
692 porewater sulfide concentrations and sulfide transport out of sediment at this site (Roden and  
693 Tuttle 1993). Sulfur cycling organisms, especially sulfate reducing Deltaproteobacteria, and the  
694 sulfur oxidizing and purple sulfur bacteria from the Gammaproteobacteria, were found  
695 associated with large particles. The exception was purple nonsulfur bacteria which were found  
696 to be free-living. Purple sulfur bacteria are large, with a width of around 4  $\mu\text{m}$  (Madigan and  
697 Martinko 2005), and so their presence in the 1.2 – 5  $\mu\text{m}$  size fraction could indicate that these  
698 organisms were free-living when found in that size fraction. However, these purple sulfur  
699 bacteria were also found in the larger size fractions suggesting they were also particle  
700 associated. Several ASVs of sulfate reducing Desulfobacteraceae and Desulfobaeae were  
701 associated with intermediate particle size fractions at station CB3.2, rather than the smallest  
702 particle size fraction. This pattern is unusual since most ASVs are primarily on the small size  
703 fractions, as discussed above. Therefore, this abundance on intermediate particles suggests  
704 that these bacteria, at least at station CB3.2, have intermediate particles as their primary  
705 habitat. It has been suggested that large particles may be sites of sulfate reduction because  
706 reductants are abundant and other oxidants such as nitrate, nitrite and oxygen cannot diffuse  
707 into the particle cores (Bianchi et al. 2018) and sulfate reducers and sulfate reduction have been  
708 found on particles previously (Fuchsman et al. 2012; Saunders et al. 2019; Raven et al. 2021).  
709 Such a pattern then suggests the presence of anoxic environments in these large particles

710 which may be leveraged by sulfate reducing bacteria. However, the association of sulfate  
711 reducers primarily with the smallest particle size fraction at the other stations suggests a more  
712 complex pattern.

### 713 Methodological Considerations

714 Our method worked well to quantitatively measure microbial community structure along a  
715 particle size gradient, across the surface and deep waters of the Chesapeake Bay. However,  
716 there are some important methodological considerations intrinsic to this approach. Most of these  
717 are not unique to our study, but rather affect microbial community studies in general, but warrant  
718 consideration here. The considerations are that some bacteria are large, some particles are  
719 fragile, some bacteria contain multiple copies of marker genes, and that Illumina read quality  
720 was comparatively lower for this project than in other amplicon studies. Large Bacteria: Some  
721 bacterial taxa exceed 1.2  $\mu\text{m}$  in width and so may show up in the 1.2 – 5  $\mu\text{m}$  bin. However, our  
722 primary conclusions hold even if we only consider bacteria in the 5  $\mu\text{m}$  and larger (Figure  
723 S12A,B). Fragile Particles: The delicate nature of particles introduces the risk of disaggregation  
724 during gravity filtration, potentially skewing the particle size to mass spectrum and reassigning  
725 cells to smaller size fractions. Filter Handling: Despite precautions, including frequent rinsing of  
726 filters, there is a potential for filter clogging and bacterial aggregation during filtration, especially  
727 for the smaller mesh sizes, potentially leading to misrepresentation of bacterial abundance and  
728 community structure in some size categories. Genetic markers: Many bacteria contain multiple  
729 (between 1 and 15) copies of the 16S gene (Venter et al. 2004; Espejo and Plaza 2018) and  
730 eukaryotes even more copies of the 18S gene (Fuchsman et al. 2022 and references therein),  
731 which inflate gene copy counts and skew proportions towards bacteria with more 16S gene  
732 copies. Microscopy validation indicates that our DNA-based methods are realistic, though higher  
733 on average than microscopy counts (Figure S8). DNA Extraction Efficiency: Our assumption of  
734 100% DNA extraction efficiency (Eqn. 2). may lead to underestimates of the abundance of some  
735 taxa (Han et al. 2018; Nearing et al. 2021; Brauer and Bengtsson 2022). Adding spikes before  
736 DNA extraction (following Gifford et al. 2020) could correct for this loss, but was not done here.  
737 Amplification Bias: The PCR step of amplicon sequencing may preferentially amplify some  
738 organisms (Elbrecht and Leese 2015). While our primer set has been validated and shows  
739 minimal bias, it does not capture all bacterial clades (McNichol et al. 2021). Read Quality  
740 Issues: Our lower than typical read quality (Lee 2019) might have adversely impacted accuracy  
741 (see Results, Amplicon Processing and Figure S7A-D). However, similarities in richness  
742 between different sequencing runs affirms that read quality does not substantially affect our  
743 results. Despite this, the presence of low read number ASVs could artificially increase perceived  
744 diversity. Low Read Depth Samples: We included three samples with low read depth (< 1300  
745 reads, after processing), as they provided information about community structure. While they  
746 may have introduced inaccuracies in some of our ordination analyses, we used diversity index  
747 statistics that were robust to the low read depths.

### 748 Additional points of discussion

749 Samples of free-living and small particle associated microorganisms appear to vary  
750 more with temperature and salinity than microorganisms that are associated with larger particles  
751 (Figure 3). One possible reason for this greater similarity between large particle samples is that  
752 microbial niches on large particles might be defined more by the properties of the particle to

753 which they are attached than to the surrounding water. Meanwhile free-living bacteria have the  
754 water itself as their habitat and small particle-attached bacteria may experience conditions  
755 intermediate to those of free-living bacteria and those attached to large particles – for instance  
756 they likely have some of the chemical substrates and physical attachment surfaces in common  
757 with large particle-attached bacteria, but exposure to oxygen or other oxidants more like those  
758 of free-living bacteria. Previous analysis has shown similarity of microbes on particles across  
759 depths in the oligotrophic ocean and much of that was attributed to particle movement between  
760 environments (Mestre et al. 2018), which could also be a factor here.

761 While we found that microbial abundance scales with particle mass, we did not try to  
762 normalize to particle surface area. This is because marine snow are believed to have shapes  
763 that are closer to fractals than spheres, with substantial folding and pore space (Logan and  
764 Wilkinson 1990; Dissanayake et al. 2018). Thus, they have surface areas much higher than for  
765 equivalently sized spheres. Furthermore, bacteria are found throughout particles (Flintrop et al.  
766 2018). Thus, we contend that it is reasonable that microbial abundance scales with particle  
767 volume, which, assuming that the volume of the non-porous portion of the particle scales with  
768 mass (as in Cram et al. 2018), means that microbial abundance should also scale with mass.

## 769 **Conclusion**

770 This work extends our knowledge of microbial biogeography in the Chesapeake Bay from an  
771 analysis of spatial and depth variability into one that concurrently considers variability of habitats  
772 within locations. We show that such within-location habitat variability is important and that  
773 bacteria have niches that are defined not only by geography, but also particle size. Bacteria  
774 involved in sulfur and methane cycling appear to associate with intermediate particle size  
775 classes, suggesting that select particles provide sites for water column biogeochemical  
776 transformations that often occur in anoxic environments. Extending this approach to consider  
777 bacterial biogeography within habitats in more regions, and across more kinds of microhabitats  
778 will provide new understanding of the ecological niches of marine microorganisms.

## 779 **Data Availability Statement**

780 Sequence data are available on NCBI's Short read archive under accession number  
781 PRJNA898904 "Chesapeake Bay 2019 Particle Size Fractionation." The amplicon sequencing  
782 pipeline, applied to the raw sequence data and which generates the microbial read counts and  
783 taxonomy is archived and publicly available on FigShare  
784 <https://doi.org/10.6084/m9.figshare.21950354.v1>. Data analysis scripts used to generate all  
785 figures and tables are also on FigShare <https://doi.org/10.6084/m9.figshare.21948425.v2>.

## 786 **Acknowledgements**

787 The authors thank Sairah Malkin, Mekayla Reynolds, Emily Dougherty and the Captain and  
788 crew of the UMCES RV *Rachael Carson* for their help with field collection; Sabeena Nazar and  
789 Allan Place for their assistance with sequencing; Michael Lee and Chris Trivedi for guidance in  
790 amplicon sequence data processing; and Larry Sanford for useful feedback regarding  
791 methodology. Ryan Moore provided insight about alpha diversity measurement. Jeff Cornwell  
792 and Michael Owens produced the hydrogen sulfide profile at station CB4.3C. James Pierson  
793 and Catherine Fitzgerald provided helpful insight about the taxonomy ecology and development  
794 of mesoplankton, especially *Acartia tonsa*. João Maia designed the graphical abstract. The

795 authors are thankful for the Startup funds provided to Cram and Fuchsman by UMCES Horn  
796 Point Laboratory. G. Martinez was funded by the Maryland Sea Grant REU program which in  
797 turn was funded by NSF grant OCE-1756244.

## 798 **References**

- 799 Alldredge AL, Cole JJ, Caron DA. Production of heterotrophic bacteria inhabiting macroscopic  
800 organic aggregates(marine snow) from surface waters. *Limnol Oceanogr.*  
801 1986;31(1):68–78.
- 802 Alldredge AL, Gotschalk C. In situ settling behavior of marine snow. *Limnol Oceanogr.* 1988  
803 May 1;33(3):339–51.
- 804 Alldredge AL, Silver MW. Characteristics, dynamics and significance of marine snow. *Prog*  
805 *Oceanogr.* 1988;20(1):41–82.
- 806 Amin SA, Hmelo LR, van Tol HM, Durham BP, Carlson LT, Heal KR, et al. Interaction and  
807 signalling between a cosmopolitan phytoplankton and associated bacteria. *Nature.* 2015  
808 Jun;522(7554):98–101.
- 809 Arora-Williams K, Holder C, Secor M, Ellis H, Xia M, Gnanadesikan A, et al. Abundant and  
810 persistent sulfur-oxidizing microbial populations are responsive to hypoxia in the  
811 Chesapeake Bay. *Environ Microbiol* [Internet]. 2022 [cited 2022 Apr 6];00(00). Available  
812 from: <http://onlinelibrary.wiley.com/doi/abs/10.1111/1462-2920.15976>
- 813 Arthur MA, Dean WE, Claypool GE. Anomalous  $^{13}\text{C}$  enrichment in modern marine organic  
814 carbon. *Nature.* 1985 May;315(6016):216–8.
- 815 Azam F, Malfatti F. Microbial structuring of marine ecosystems. *Nat Rev Microbiol.* 2007  
816 Oct;5(10):782–91.
- 817 Barbera P, Kozlov AM, Czech L, Morel B, Darriba D, Flouri T, et al. EPA-ng: Massively Parallel  
818 Evolutionary Placement of Genetic Sequences. *Syst Biol.* 2019 Mar 1;68(2):365–9.
- 819 Baross J, Crump B, Simenstad C. Elevated 'microbial loop' activities in the Columbia River  
820 estuary turbidity maximum. In: *Changing Particle Fluxes in Estuaries: Implications from*  
821 *Science to Management.* 1994. p. 459–64.
- 822 Bertagnolli AD, Konstantinidis KT, Stewart FJ. Non-denitrifier nitrous oxide reductases dominate  
823 marine biomes. *Environ Microbiol Rep.* 2020;12(6):681–92.
- 824 Bianchi D, Weber TS, Kiko R, Deutsch C. Global niche of marine anaerobic metabolisms  
825 expanded by particle microenvironments. *Nat Geosci.* 2018 Apr;11(4):263.
- 826 Bidle KD, Fletcher M. Comparison of free-living and particle-associated bacterial communities in  
827 the chesapeake bay by stable low-molecular-weight RNA analysis. *Appl Environ*  
828 *Microbiol.* 1995;61(3):944–52.
- 829 Boyd CE. Hydrogen Sulfide Toxic, But Manageable. *Glob Aquac Advocate.* 2014;34–6.
- 830 Brauer A, Bengtsson MM. DNA extraction bias is more pronounced for microbial eukaryotes  
831 than for prokaryotes. *MicrobiologyOpen.* 2022;11(5):e1323.

832 Callahan BJ, McMurdie PJ, Rosen MJ, Han AW, Johnson AJA, Holmes SP. DADA2: High-  
833 resolution sample inference from Illumina amplicon data. *Nat Methods*. 2016  
834 Jul;13(7):581–3.

835 Colwell RR, Kaper J, Joseph SW. *Vibrio cholerae*, *Vibrio parahaemolyticus*, and Other *Vibrios*:  
836 Occurrence and Distribution in Chesapeake Bay. *Science*. 1977 Oct 28;198(4315):394–  
837 6.

838 Coolen MJL, Abbas B, Van Bleijswijk J, Hopmans EC, Kuypers MMM, Wakeham SG, et al.  
839 Putative ammonia-oxidizing Crenarchaeota in suboxic waters of the Black Sea: a basin-  
840 wide ecological study using 16S ribosomal and functional genes and membrane lipids.  
841 *Environ Microbiol*. 2007;9(4):1001–16.

842 Cram JA, Chow CET, Sachdeva R, Needham DM, Parada AE, Steele JA, et al. Seasonal and  
843 interannual variability of the marine bacterioplankton community throughout the water  
844 column over ten years. *ISME J*. 2015;9:563–80.

845 Cram JA, Parada AE, Fuhrman JA. Dilution reveals how viral lysis and grazing shape microbial  
846 communities: Viral Lysis and Grazing Shape Microbial Communities. *Limnol Oceanogr*.  
847 2016 Feb;61(3):889–905.

848 Cram JA, Weber T, Leung SW, McDonnell AMP, Liang JH, Deutsch C. The Role of Particle  
849 Size, Ballast, Temperature, and Oxygen in the Sinking Flux to the Deep Sea. *Glob*  
850 *Biogeochem Cycles*. 2018 May;32(5):858–76.

851 Crump BC, Peranteau C, Beckingham B, Cornwell JC. Respiratory Succession and Community  
852 Succession of Bacterioplankton in Seasonally Anoxic Estuarine Waters. *Appl Environ*  
853 *Microbiol*. 2007 Nov 1;73(21):6802–10.

854 Cruz BN, Neuer S. Heterotrophic Bacteria Enhance the Aggregation of the Marine  
855 Picocyanobacteria *Prochlorococcus* and *Synechococcus*. *Front Microbiol*. 2019 Aug  
856 13;10:1864.

857 Czech L, Barbera P, Stamatakis A. Genesis and Gappa: processing, analyzing and visualizing  
858 phylogenetic (placement) data. *Bioinformatics*. 2020 May 1;36(10):3263–5.

859 DeLong EF, Franks DG, Alldredge AL. Phylogenetic diversity of aggregate-attached vs. free-  
860 living marine bacterial assemblages. *Limnol Oceanogr*. 1993;38(5):924–34.

861 DeVries T, Liang JH, Deutsch C. A mechanistic particle flux model applied to the oceanic  
862 phosphorus cycle. *Biogeosciences Discuss*. 2014 Mar 6;11(3):3653–99.

863 Dissanayake AL, Burd AB, Daly KL, Francis S, Passow U. Numerical Modeling of the  
864 Interactions of Oil, Marine Snow, and Riverine Sediments in the Ocean. *J Geophys Res*  
865 *Oceans*. 2018;123(8):5388–405.

866 Dougherty E, Cram J, Hollins A. The relationship between size, abundance, and mass of  
867 particles in the surface and bottom waters of the Chesapeake Bay [Internet].  
868 *Oceanography*; 2021 Oct. Available from:  
869 <http://www.essoar.org/doi/10.1002/essoar.10508364.1>

- 870 Douglas GM, Maffei VJ, Zaneveld JR, Yurgel SN, Brown JR, Taylor CM, et al. PICRUSt2 for  
871 prediction of metagenome functions. *Nat Biotechnol.* 2020 Jun;38(6):685–8.
- 872 Elbrecht V, Leese F. Can DNA-Based Ecosystem Assessments Quantify Species Abundance?  
873 Testing Primer Bias and Biomass—Sequence Relationships with an Innovative  
874 Metabarcoding Protocol. Hajjibabaei M, editor. *PLOS ONE.* 2015 Jul 8;10(7):e0130324.
- 875 Espejo RT, Plaza N. Multiple Ribosomal RNA Operons in Bacteria; Their Concerted Evolution  
876 and Potential Consequences on the Rate of Evolution of Their 16S rRNA. *Front*  
877 *Microbiol.* 2018;9:1232.
- 878 Farnelid H, Turk-Kubo K, Ploug H, Ossolinski JE, Collins JR, Mooy BASV, et al. Diverse  
879 diazotrophs are present on sinking particles in the North Pacific Subtropical Gyre. *ISME*  
880 *J.* 2018 Aug 16;1.
- 881 Findlay AJ, Bennett AJ, Hanson TE, Luther GW. Light-Dependent Sulfide Oxidation in the  
882 Anoxic Zone of the Chesapeake Bay Can Be Explained by Small Populations of  
883 Phototrophic Bacteria. *Appl Environ Microbiol.* 2015 Nov;81(21):7560–9.
- 884 Flintrop CM, Rogge A, Miksch S, Thiele S, Waite AM, Iversen MH. Embedding and slicing of  
885 intact in situ collected marine snow: Embedding and slicing of marine snow. *Limnol*  
886 *Oceanogr Methods.* 2018 Jun;16(6):339–55.
- 887 Fortunato CS, Herfort L, Zuber P, Baptista AM, Crump BC. Spatial variability overwhelms  
888 seasonal patterns in bacterioplankton communities across a river to ocean gradient.  
889 *ISME J.* 2011;6(3):554–63.
- 890 Froelich B, Ayrapetyan M, Oliver JD. Integration of *Vibrio vulnificus* into Marine Aggregates and  
891 Its Subsequent Uptake by *Crassostrea virginica* Oysters. *Appl Environ Microbiol.* 2013  
892 Mar;79(5):1454–8.
- 893 Fuchsman CA, Cherubini L, Hays MD. An analysis of protists in Pacific oxygen deficient zones:  
894 implications for *Prochlorococcus* and N<sub>2</sub>-producing bacteria. *Environ Microbiol.* 2022  
895 Apr;24(4):1790–804.
- 896 Fuchsman CA, Devol AH, Saunders JK, McKay C, Rocap G. Niche Partitioning of the N Cycling  
897 Microbial Community of an Offshore Oxygen Deficient Zone. *Front Microbiol* [Internet].  
898 2017 Dec 5 [cited 2018 Dec 4];8. Available from:  
899 <http://journal.frontiersin.org/article/10.3389/fmicb.2017.02384/full>
- 900 Fuchsman CA, Murray JW, Staley JT. Stimulation of Autotrophic Denitrification by Intrusions of  
901 the Bosphorus Plume into the Anoxic Black Sea. *Front Microbiol* [Internet]. 2012 [cited  
902 2019 Jul 6];3. Available from:  
903 <https://www.frontiersin.org/articles/10.3389/fmicb.2012.00257/full>
- 904 Fuchsman CA, Palevsky HI, Widner B, Duffy M, Carlson MCG, Neibauer JA, et al.  
905 Cyanobacteria and cyanophage contributions to carbon and nitrogen cycling in an  
906 oligotrophic oxygen-deficient zone. *ISME J.* 2019a Jun 27;1.

- 907 Fuchsman CA, Paul B, Staley JT, Yakushev EV, Murray JW. Detection of Transient  
908 Denitrification During a High Organic Matter Event in the Black Sea. *Glob Biogeochem*  
909 *Cycles*. 2019b;33(2):143–62.
- 910 Fuhrman JA, Comeau DE, Hagström AÅke, Chan AM. Extraction from natural planktonic  
911 microorganisms of DNA suitable for molecular biological studies. *Appl Environ Microbiol*.  
912 1988;54(6):1426–9.
- 913 Ganesh S, Parris DJ, DeLong EF, Stewart FJ. Metagenomic analysis of size-fractionated  
914 picoplankton in a marine oxygen minimum zone. *ISME J*. 2014 Jan;8(1):187–211.
- 915 Garcia JL, Patel BKC, Ollivier B. Taxonomic, Phylogenetic, and Ecological Diversity of  
916 Methanogenic Archaea. *Anaerobe*. 2000 Aug 1;6(4):205–26.
- 917 Gelesh L, Marshall K, Boicourt W, Lapham L. Methane concentrations increase in bottom  
918 waters during summertime anoxia in the highly eutrophic estuary, Chesapeake Bay,  
919 U.S.A. *Limnol Oceanogr*. 2016;61(S1):S253–66.
- 920 Geyer WR. The Importance of Suppression of Turbulence by Stratification on the Estuarine  
921 Turbidity Maximum. *Estuaries*. 1993 Mar;16(1):113.
- 922 Gifford SM, Zhao L, Stemple B, DeLong K, Medeiros PM, Seim H, et al. Microbial Niche  
923 Diversification in the Galápagos Archipelago and Its Response to El Niño. *Front*  
924 *Microbiol* [Internet]. 2020 [cited 2022 Jul 11];11. Available from:  
925 <https://www.frontiersin.org/articles/10.3389/fmicb.2020.575194>
- 926 Giovannoni SJ, Tripp HJ, Givan S, Podar M, Vergin KL, Baptista D, et al. Genome Streamlining  
927 in a Cosmopolitan Oceanic Bacterium. *Science*. 2005 Aug 19;309(5738):1242–5.
- 928 Hagen RA, Vogt PR. Seasonal variability of shallow biogenic gas in Chesapeake Bay. *Mar*  
929 *Geol*. 1999 Jun 1;158(1):75–88.
- 930 Han Z, Sun J, Lv A, Wang A. Biases from different DNA extraction methods in intestine  
931 microbiome research based on 16S rDNA sequencing: a case in the koi carp, *Cyprinus*  
932 *carpio* var. *Koi*. *MicrobiologyOpen*. 2018 Apr 17;8(1):e00626.
- 933 Harker M, Hirschberg J, Oren A 1998. *Paracoccus marcusii* sp. nov., an orange Gram-negative  
934 coccus. *Int J Syst Evol Microbiol*. 1998;48(2):543–8.
- 935 Ji Q, Frey C, Sun X, Jackson M, Lee YS, Jayakumar A, et al. Nitrogen and oxygen availabilities  
936 control water column nitrous oxide production during seasonal anoxia in the  
937 Chesapeake Bay. *Biogeosciences*. 2018 Oct 18;15(20):6127–38.
- 938 Johansson ON, Pinder MIM, Ohlsson F, Egardt J, Töpel M, Clarke AK. Friends With Benefits:  
939 Exploring the Phycosphere of the Marine Diatom *Skeletonema marinoi*. *Front Microbiol*  
940 [Internet]. 2019 [cited 2022 Oct 25];10. Available from:  
941 <https://www.frontiersin.org/articles/10.3389/fmicb.2019.01828>
- 942 Kan J, Crump BC, Wang K, Chen F. Bacterioplankton community in Chesapeake Bay:  
943 Predictable or random assemblages. *Limnol Oceanogr*. 2006 Sep;51(5):2157–69.

- 944 Kan J, Suzuki MT, Wang K, Evans SE, Chen F. High Temporal but Low Spatial Heterogeneity  
945 of Bacterioplankton in the Chesapeake Bay. *Appl Environ Microbiol.* 2007 Nov  
946 1;73(21):6776–89.
- 947 Kanehisa M. Enzyme Annotation and Metabolic Reconstruction Using KEGG. *Methods Mol Biol*  
948 Clifton NJ. 2017;1611:135–45.
- 949 Kaneko T, Colwell RR. Ecology of *Vibrio parahaemolyticus* in Chesapeake Bay. *J Bacteriol.*  
950 1973 Jan;113(1):24–32.
- 951 Kang JC. Acute toxicity of hydrogen sulfide to larvae and adults of blue crab *Portunus*  
952 *trituberculatus* white shrimp *Metapenaeus monoceros* and prawn *Macrobrachium*  
953 *nipponens*. *J Fish Pathol.* 1997;10(1):65–72.
- 954 Kimmel DG, Roman MR, Zhang X. Spatial and temporal variability in factors affecting  
955 mesozooplankton dynamics in Chesapeake Bay: Evidence from biomass size spectra.  
956 *Limnol Oceanogr.* 2006 Jan;51(1):131–41.
- 957 Kiørboe T, Tang K, Grossart HP, Ploug H. Dynamics of Microbial Communities on Marine Snow  
958 Aggregates: Colonization, Growth, Detachment, and Grazing Mortality of Attached  
959 Bacteria. *Appl Environ Microbiol.* 2003 Jun 1;69(6):3036–47.
- 960 Kirstein IV, Kirmizi S, Wichels A, Garin-Fernandez A, Erler R, Löder M, et al. Dangerous  
961 hitchhikers? Evidence for potentially pathogenic *Vibrio* spp. on microplastic particles.  
962 *Mar Environ Res.* 2016 Sep 1;120:1–8.
- 963 Laperriere SM, Nidziko NJ, Fox RJ, Fisher AW, Santoro AE. Observations of Variable  
964 Ammonia Oxidation and Nitrous Oxide Flux in a Eutrophic Estuary. *Estuaries Coasts.*  
965 2019 Jan 1;42(1):33–44.
- 966 Lee D, Keller D, Crump B, Hood R. Community metabolism and energy transfer in the  
967 Chesapeake Bay estuarine turbidity maximum. *Mar Ecol Prog Ser.* 2012 Mar 8;449:65–  
968 82.
- 969 Lee M. Happy Belly Bioinformatics: an open-source resource dedicated to helping biologists  
970 utilize bioinformatics. *J Open Source Educ.* 2019 Sep 29;2(19):53.
- 971 Leu AO, Eppley JM, Burger A, DeLong EF. Diverse Genomic Traits Differentiate Sinking-  
972 Particle-Associated versus Free-Living Microbes throughout the Oligotrophic Open  
973 Ocean Water Column. Bello MGD, editor. *mBio.* 2022 Jul 12;e01569-22.
- 974 Liang J, Liu J, Wang X, Lin H, Liu J, Zhou S, et al. Spatiotemporal Dynamics of Free-Living and  
975 Particle-Associated *Vibrio* Communities in the Northern Chinese Marginal Seas. *Appl*  
976 *Environ Microbiol.* 2019 Apr 18;85(9):e00217-19.
- 977 Logan BE, Wilkinson DB. Fractal geometry of marine snow and other biological aggregates.  
978 *Limnol Oceanogr.* 1990;35(1):130–6.
- 979 Long RA, Azam F. Microscale patchiness of bacterioplankton assemblage richness in seawater.  
980 *Aquat Microb Ecol.* 2001 Dec 5;26(2):103–13.

- 981 Louca S, Doebeli M. Efficient comparative phylogenetics on large trees. *Bioinformatics*. 2018  
982 Mar 15;34(6):1053–5.
- 983 MacArthur RH, Wilson EO. *The theory of island biogeography*. Princeton: Princeton University  
984 Press; 2001.
- 985 Madigan MT, Martinko JM. *Brock Biology Of Microorganisms 11th EDITION*. 11th ed. Lebanon,  
986 Indiana, U.S.A.: Pren; 2005.
- 987 Malpezzi MA, Sanford LP, Crump BC. Abundance and distribution of transparent exopolymer  
988 particles in the estuarine turbidity maximum of Chesapeake Bay. *Mar Ecol Prog Ser*.  
989 2013;486:23–35.
- 990 McNichol J, Berube PM, Biller SJ, Fuhrman JA. Evaluating and Improving Small Subunit rRNA  
991 PCR Primer Coverage for Bacteria, Archaea, and Eukaryotes Using Metagenomes from  
992 Global Ocean Surveys. *mSystems*. 2021 Jun 29;6(3):e0056521.
- 993 Mestre M, Borrull E, Sala Mm, Gasol JM. Patterns of bacterial diversity in the marine planktonic  
994 particulate matter continuum. *ISME J*. 2017 Apr;11(4):999–1010.
- 995 Mestre M, Höfer J, Sala MM, Gasol JM. Seasonal Variation of Bacterial Diversity Along the  
996 Marine Particulate Matter Continuum. *Front Microbiol* [Internet]. 2020 [cited 2022 Jun  
997 2];11. Available from: <https://www.frontiersin.org/article/10.3389/fmicb.2020.01590>
- 998 Mestre M, Ruiz-González C, Logares R, Duarte CM, Gasol JM, Sala MM. Sinking particles  
999 promote vertical connectivity in the ocean microbiome. *Proc Natl Acad Sci*. 2018 Jun  
1000 27;201802470.
- 1001 Montagna M, Sasseria D, Epis S, Bazzocchi C, Vannini C, Lo N, et al. “Candidatus  
1002 Midichloriaceae” fam. nov. (Rickettsiales), an Ecologically Widespread Clade of  
1003 Intracellular Alphaproteobacteria. *Appl Environ Microbiol*. 2013 May;79(10):3241–8.
- 1004 Nearing JT, Comeau AM, Langille MGI. Identifying biases and their potential solutions in human  
1005 microbiome studies. *Microbiome*. 2021 May 18;9(1):113.
- 1006 Needham D, Fichot E, Parada A, Yeh YC, Fuhrman J. Fuhrman Lab 515F-926R16S and 18S  
1007 rRNA Gene Sequencing Protocol v2 [Internet]. 2018 Nov. Available from:  
1008 [https://www.protocols.io/view/fuhrman-lab-515f-926r-16s-and-18s-rrna-gene-sequen-  
1009 vb7e2rn](https://www.protocols.io/view/fuhrman-lab-515f-926r-16s-and-18s-rrna-gene-sequen-vb7e2rn)
- 1010 Oksanen J, Blanchet FG, Kindt R, Legendre P, Minchin PR, O’Hara RB, et al. *vegan*:  
1011 Community Ecology Package [Internet]. 2013. Available from: [http://CRAN.R-  
1012 project.org/package=vegan](http://CRAN.R-project.org/package=vegan)
- 1013 Palinkas CM, Testa JM, Cornwell JC, Li M, Sanford LP. Influences of a River Dam on Delivery  
1014 and Fate of Sediments and Particulate Nutrients to the Adjacent Estuary: Case Study of  
1015 Conowingo Dam and Chesapeake Bay. *Estuaries Coasts*. 2019 Dec 1;42(8):2072–95.
- 1016 Phillips CJ, Smith Z, Embley TM, Prosser JI. Phylogenetic Differences between Particle-  
1017 Associated and Planktonic Ammonia-Oxidizing Bacteria of the  $\beta$  Subdivision of the Class

- 1018 Proteobacteria in the Northwestern Mediterranean Sea. *Appl Environ Microbiol.* 1999  
1019 Feb;65(2):779–86.
- 1020 Ploug H, Kühl M, Buchholz B, Jørgensen BB. Anoxic aggregates an ephemeral phenomenon in  
1021 the ocean. *Aquat Microb Ecol.* 1997;13:285–94.
- 1022 Quast C, Pruesse E, Yilmaz P, Gerken J, Schweer T, Yarza P, et al. The SILVA ribosomal RNA  
1023 gene database project: improved data processing and web-based tools. *Nucleic Acids*  
1024 *Res.* 2013 Jan 1;41(D1):D590–6.
- 1025 Rappé MS, Connon SA, Vergin KL, Giovannoni SJ. Cultivation of the ubiquitous SAR11 marine  
1026 bacterioplankton clade. *Nature.* 2002 Aug;418(6898):630–3.
- 1027 Raven MR, Keil RG, Webb SM. Microbial sulfate reduction and organic sulfur formation in  
1028 sinking marine particles. *Science.* 2021 Jan 8;371(6525):178–81.
- 1029 Reeburgh WS. Observations of Gases in Chesapeake Bay Sediments<sup>1</sup>. *Limnol Oceanogr.*  
1030 1969;14(3):368–75.
- 1031 Rieck A, Herlemann DPR, Jürgens K, Grossart HP. Particle-Associated Differ from Free-Living  
1032 Bacteria in Surface Waters of the Baltic Sea. *Front Microbiol [Internet].* 2015 [cited 2022  
1033 Nov 8];6. Available from: <https://www.frontiersin.org/articles/10.3389/fmicb.2015.01297>
- 1034 Roden EE, Tuttle JH. Sulfide release from estuarine sediments underlying anoxic bottom water.  
1035 *Limnol Oceanogr.* 1992;37(4):725–38.
- 1036 Roden EE, Tuttle JH. Inorganic sulfur turnover in oligohaline estuarine sediments.  
1037 *Biogeochemistry.* 1993 Jun;22(2):81–105.
- 1038 Ruppert EE, Fox RS, Barnes RD. *Invertebrate zoology: a functional evolutionary approach.* 7th  
1039 ed. Belmont, CA: Thomson-Brooks/Cole; 2004.
- 1040 Sanford LP, Suttles SE, Halka JP. Reconsidering the physics of the Chesapeake Bay estuarine  
1041 turbidity maximum. *Estuaries.* 2001 Oct 1;24(5):655–69.
- 1042 Saunders JK, Fuchsman CA, McKay C, Rocard G. Complete arsenic-based respiratory cycle in  
1043 the marine microbial communities of pelagic oxygen-deficient zones. *Proc Natl Acad Sci.*  
1044 2019 May 14;116(20):9925–30.
- 1045 Schubel JR. Turbidity maximum of the northern Chesapeake Bay. *Science.*  
1046 1968;161(3845):1013–5.
- 1047 Shibata A, Kogure K, Koike I, Ohwada K. Formation of submicron colloidal particles from marine  
1048 bacteria by viral infection. *Mar Ecol Prog Ser.* 1997;155:303–7.
- 1049 Shibl AA, Isaac A, Ochsenkühn MA, Cárdenas A, Fei C, Behringer G, et al. Diatom modulation  
1050 of select bacteria through use of two unique secondary metabolites. *Proc Natl Acad Sci.*  
1051 2020 Nov 3;117(44):27445–55.
- 1052 Shu Q. Molecular progresses of marine Planctomycetes: A review. *Afr J Microbiol Res*  
1053 [Internet]. 2011 Dec 31 [cited 2023 Oct 26];5(33). Available from:

- 1054 [http://www.academicjournals.org/AJMR/abstracts/abstract%202011/December](http://www.academicjournals.org/AJMR/abstracts/abstract%202011/December%20Special%20Review/Shu%20et%20al.htm)  
1055 [%20Special%20Review/Shu%20et%20al.htm](http://www.academicjournals.org/AJMR/abstracts/abstract%202011/December%20Special%20Review/Shu%20et%20al.htm)
- 1056 Simon M, Alldredge A, Azam F. Bacterial carbon dynamics on marine snow. *Mar Ecol Prog Ser.*  
1057 1990;65:205–11.
- 1058 Simon M, Grossart H, Schweitzer B, Ploug H. Microbial ecology of organic aggregates in  
1059 aquatic ecosystems. *Aquat Microb Ecol.* 2002 Jun 26;28(2):175–211.
- 1060 Stief P, Kamp A, Thamdrup B, Glud RN. Anaerobic Nitrogen Turnover by Sinking Diatom  
1061 Aggregates at Varying Ambient Oxygen Levels. *Front Microbiol* [Internet]. 2016 Feb 5  
1062 [cited 2019 Jul 31];7. Available from:  
1063 <http://journal.frontiersin.org/Article/10.3389/fmicb.2016.00098/abstract>
- 1064 Stocker R. Marine Microbes See a Sea of Gradients. *Science.* 2012 Nov 1;338(6107):628–33.
- 1065 Tee HS, Waite D, Lear G, Handley KM. Microbial river-to-sea continuum: gradients in benthic  
1066 and planktonic diversity, osmoregulation and nutrient cycling. *Microbiome.* 2021 Sep  
1067 20;9(1):190.
- 1068 Testa JM, Kemp WM, Boynton WR. Season-specific trends and linkages of nitrogen and oxygen  
1069 cycles in Chesapeake Bay: Linked oxygen and nitrogen trends. *Limnol Oceanogr*  
1070 [Internet]. 2018 May 31 [cited 2018 Oct 18]; Available from:  
1071 <http://doi.wiley.com/10.1002/lno.10823>
- 1072 Tourlousse DM, Yoshiike S, Ohashi A, Matsukura S, Noda N, Sekiguchi Y. Synthetic spike-in  
1073 standards for high-throughput 16S rRNA gene amplicon sequencing. *Nucleic Acids Res.*  
1074 2017 Feb 28;45(4):e23.
- 1075 Trojan D, Schreiber L, Bjerg JT, Bøggild A, Yang T, Kjeldsen KU, et al. A taxonomic framework  
1076 for cable bacteria and proposal of the candidate genera *Electrothrix* and *Electronema*.  
1077 *Syst Appl Microbiol.* 2016 Jul 1;39(5):297–306.
- 1078 Tsubokura A, Yoneda H, Mizuta H 1999. *Paracoccus carotinifaciens* sp. nov., a new aerobic  
1079 Gram-negative astaxanthin-producing bacterium. *Int J Syst Evol Microbiol.*  
1080 1999;49(1):277–82.
- 1081 Turk V, Malkin SY, Celussi M, Tinta T, Cram J, Malfatti F, et al. Ecological Role of Microbes:  
1082 Current Knowledge and Future Prospects. In: Malone TC, Malej A, Faganeli J, editors.  
1083 Coastal Ecosystems in Transition: A Comparative Analysis of the Northern Adriatic and  
1084 Chesapeake Bay. John Wiley & Sons; 2021.
- 1085 Turner JS, St-Laurent P, Friedrichs MAM, Friedrichs CT. Effects of reduced shoreline erosion  
1086 on Chesapeake Bay water clarity. *Sci Total Environ.* 2021 May 15;769:145157.
- 1087 Vanwonterghem I, Evans PN, Parks DH, Jensen PD, Woodcroft BJ, Hugenholtz P, et al.  
1088 Methylophilic methanogenesis discovered in the archaeal phylum Verstraetearchaeota.  
1089 *Nat Microbiol.* 2016 Dec;1(12):16170.

- 1090 Venter JC, Remington K, Heidelberg JF, Halpern AL, Rusch D, Eisen JA, et al. Environmental  
1091 Genome Shotgun Sequencing of the Sargasso Sea. *Science*. 2004 Apr 2;304(5667):66–  
1092 74.
- 1093 Větrovský T, Baldrian P. The Variability of the 16S rRNA Gene in Bacterial Genomes and Its  
1094 Consequences for Bacterial Community Analyses. *PLoS ONE*. 2013 Feb  
1095 27;8(2):e57923.
- 1096 Wang H, Zhang C, Chen F, Kan J. Spatial and temporal variations of bacterioplankton in the  
1097 Chesapeake Bay: A re-examination with high-throughput sequencing analysis. *Limnol  
1098 Oceanogr*. 2020;65(12):3032–45.
- 1099 Wang J, Hood RR. Modeling the Origin of the Particulate Organic Matter Flux to the Hypoxic  
1100 Zone of Chesapeake Bay in Early Summer. *Estuaries Coasts* [Internet]. 2020 Jul 25  
1101 [cited 2021 Jan 27]; Available from: <http://link.springer.com/10.1007/s12237-020-00806-0>  
1102 0
- 1103 Weber T, Bianchi D. Efficient Particle Transfer to Depth in Oxygen Minimum Zones of the  
1104 Pacific and Indian Oceans. *Front Earth Sci* [Internet]. 2020 [cited 2020 Dec 23];8.  
1105 Available from: <http://www.frontiersin.org/articles/10.3389/feart.2020.00376/full>
- 1106 Willis A, Martin BD, Trinh P, Barger K, Bunge J. breakaway: Species Richness Estimation and  
1107 Modeling [Internet]. 2018. Available from: <https://adw96.github.io/breakaway/>
- 1108 Yilmaz P, Parfrey LW, Yarza P, Gerken J, Pruesse E, Quast C, et al. The SILVA and “All-  
1109 species Living Tree Project (LTP)” taxonomic frameworks. *Nucleic Acids Res*. 2014 Jan  
1110 1;42(D1):D643–8.
- 1111 Zhang Q, Blomquist JD. Watershed export of fine sediment, organic carbon, and chlorophyll-a  
1112 to Chesapeake Bay: Spatial and temporal patterns in 1984–2016. *Sci Total Environ*.  
1113 2018 Apr 1;619–620:1066–78.
- 1114 Zhang X, Roman M, Kimmel D, McGilliard C, Boicourt W. Spatial variability in plankton biomass  
1115 and hydrographic variables along an axial transect in Chesapeake Bay. *J Geophys Res*.  
1116 2006;111(C5):C05S11.
- 1117 Zhang Y, Xiao W, Jiao N. Linking biochemical properties of particles to particle-attached and  
1118 free-living bacterial community structure along the particle density gradient from  
1119 freshwater to open ocean: Linking POM to Particle-Attached and Free-Living Bacteria. *J  
1120 Geophys Res Biogeosciences*. 2016 Aug;121(8):2261–74.
- 1121 Zhao R, Hannisdal B, Mogollon JM, Jørgensen SL. Nitrifier abundance and diversity peak at  
1122 deep redox transition zones. *Sci Rep*. 2019 Jun 14;9(1):8633.
- 1123 Zimmerman AR, Canuel EA. Bulk Organic Matter and Lipid Biomarker Composition of  
1124 Chesapeake Bay Surficial Sediments as Indicators of Environmental Processes. *Estuar  
1125 Coast Shelf Sci*. 2001 Sep;53(3):319–41.
- 1126 Zumft WG. Cell Biology and Molecular Basis of Denitrification. *MICROBIOL MOL BIOL REV*.  
1127 1997;61.

1128 **Supplemental Methods**

1129 Particle Processing

1130 *Phase 1. Separation of particulate material into size classes:*

1131 Water was gravity filtered, in sequence, through nylon mesh of decreasing pore size. The  
1132 water that passed through the mesh was retained. Pore sizes were 500, 180, 53, 20, 5  $\mu\text{m}$  and  
1133 mesh diameters were  $\sim 142$  mm. After filtration, each nylon mesh was back rinsed with  $\sim 500$  ml  
1134 of prefiltered “rinse water” to produce a resuspension of particulate matter from particles from  
1135 each size class. The “rinse water” had been generated during transit by pumping surface water  
1136 in sequence through water filters of size 10, 5, 1  $\mu\text{m}$  to remove particles, followed by a 0.2  $\mu\text{m}$   
1137 filter (Pall AcroPak 1500 Capsule with a Supor Polyethersulfone membrane) capsule which  
1138 removes bacteria. After back-rinsing, the resuspended particles were split, with 45 mL saved for  
1139 microscopy,  $\sim 200$  mL used for particulate matter mass measurements and  $\sim 200$  mL for DNA  
1140 measurements. In all cases the actual volumes were carefully recorded and used for  
1141 normalization during analysis. Water that had passed through all of the filters was also saved,  
1142 45 mL preserved for microscopy,  $\sim 1$  L ml used for particulate matter mass measurements and  
1143  $\sim 1$  L ml for DNA measurements.

1144 *Phase 2: Preservation of particulate material for microscopy, POM and DNA analysis*

1145 Microscopy samples were preserved with the addition of 1 mL of saturated, 0.2  $\mu\text{m}$  filtered  
1146 formaldehyde, and stored at  $-80^\circ\text{C}$ .

1147 To collect particulate matter for mass and elemental measurements, the resuspended  
1148 particulate matter from each sample and size class was collected by vacuum filtration through a  
1149 1.2  $\mu\text{m}$  nominal pore size, 25 mm diameter, GF/C glass fiber filter (Whatman WHA1822025).  
1150 These filters had been previously pre-combusted at  $400^\circ\text{C}$ , and then pre-weighed using a  
1151 Sartorius micro balance to a precision of 1  $\mu\text{g}$ . To collect particulate matter in the 1.2 – 5  $\mu\text{m}$   
1152 range,  $\sim 500$  ml of the water that had gone through all of the nylon mesh was also collected on  
1153 the 1.2  $\mu\text{m}$  GF/C filter.

1154 To collect DNA, resuspended particulate matter from each nylon filter was filtered through a  
1155 1.2  $\mu\text{m}$  pore-size 47 mm diameter, polyethersulfone filter (Sterilitech PES1247100). DNA from  
1156 the 1.2 – 5  $\mu\text{m}$  and 0.2 – 1.2  $\mu\text{m}$  ranges were collected by passing  $\sim 1$  L of the water that had  
1157 passed through the other filters, in series, through 1.2  $\mu\text{m}$  and 0.2  $\mu\text{m}$  pore size, 47 mm  
1158 diameter, polyethersulfone filters using a peristaltic pump (1.2  $\mu\text{m}$  filter as above, 0.2  $\mu\text{m}$  filter —  
1159 Sterilitech PES0247100). All DNA filters were folded, placed in a 2 mL sterile screw-cap  
1160 cryogenic tube and flash frozen in liquid nitrogen. Samples were then stored at  $-80^\circ\text{C}$  prior to  
1161 extraction.

1162 Isotopic Analysis

1163 At the University of California Davis Stable Isotope Facility, the following protocol was followed:  
1164 Samples were combusted at  $1080^\circ\text{C}$  in a reactor packed with chromium oxide and silvered  
1165 copper oxide. Oxides were removed in a reduction reactor containing reduced copper at  $650^\circ\text{C}$ .  
1166 The liberated gases were retained in a helium carrier, which flowed through a water trap  
1167 containing magnesium perchlorate and phosphorous pentoxide. Carbon dioxide was temporarily  
1168 stored in an adsorption trap until dinitrogen gas is analyzed, and then the carbon was analyzed.

1169 Both carbon and nitrogen were quantified in an Elementar Vario EL Cube coupled with an  
1170 Isoprime VisION isotope ratio mass spectrometer. The total carbon and nitrogen content of each  
1171 filter were measured, as well as  $\delta^{13}\text{C}$  and  $\delta^{15}\text{N}$  relative to Vienna Pee Dee Belemnite and Air  
1172 standards respectively.

### 1173 Microscopy measurements of bacterial abundance

1174 In cases where particle and microbial abundance was high enough that it would be  
1175 challenging to enumerate cells directly on a microscope due to overlap between bacteria, fixed  
1176 samples were first diluted 100-fold in 0.2  $\mu\text{m}$  filtered deionized water, while in others sample  
1177 water was used directly. Microbial abundances on each particle size fraction were measured by  
1178 adding 1  $\mu\text{l}/\text{mL}$  of Triton-X-100 per mL of sample, vortexing and then sonicating the sample for  
1179 30 seconds. Samples were then collected by vacuum filtration on a 0.2  $\mu\text{m}$  pore size, 25 mm  
1180 diameter, black PCTE track etched polycarbonate filter (Thomas Scientific # 4663H09).  
1181 Samples were stained in some cases by incubating with a 20 mg/L DAPI solution for 5 minutes,  
1182 in which case the DAPI was removed by filtration and the filters placed on a microscope slide,  
1183 covered with non-fluorescent immersion oil and a coverslip. In other cases, samples were  
1184 instead stained by placing Invitrogen ProLong Gold Antifade Mountant with DAPI solution  
1185 (Fisher Scientific #P36941) under the coverslip, instead of immersion oil. The two methods gave  
1186 similar results. Microbial abundances were counted on a Zeiss Axio Imager M2 epifluorescence  
1187 microscope with a gridded eyepiece and microbial counts normalized to abundance (following  
1188 Patel et al. 2007).

### 1189 DNA Extraction

1190 Frozen samples were combined with 400  $\mu\text{L}$  lysis buffer (1% Sodium Dodecyl sulfate in filter  
1191 sterilized STE (10mM Tris-Cl, 100mM NaCl, 1mM EDTA; pH 8.0)). Samples were heated at  
1192 95  $^{\circ}\text{C}$  for two minutes, put in a bead beater (BeadBug Microtube Homoginizer), without added  
1193 beads, for 30 seconds. This process was followed by another round of heating, one more round  
1194 of beating, and a final round of heating. We then added 400  $\mu\text{L}$  of phenol-chloroform solution  
1195 (25 parts phenol solution (pH8; Sigma P4557): 24 parts chloroform (Sigma C2432); 1 part  
1196 isoamyl alcohol (Sigma W205702)). Samples then underwent one additional beating step (30  
1197 seconds). During this final beating step, the filters dissolved in the phenol solution. The sample  
1198 was then centrifuged at 13,000 g at room temperature ( $\sim 20^{\circ}\text{C}$ ) for two minutes to separate the  
1199 phenol layer from the aqueous layer. The samples were again placed in the bead beater for an  
1200 additional 30 seconds and then re-centrifuged to increase the samples' exposure to phenol  
1201 chloroform. The remaining phenol layer was viscous due to the presence of dissolved filter and  
1202 was removed with a pipette from which the end had been cut off to widen the opening. An  
1203 additional 400  $\mu\text{L}$  phenol chloroform was added, samples were vortexed for 30 seconds to mix,  
1204 the sample was re-centrifuged and the phenol again removed. Next 400  $\mu\text{L}$  of chloroform-  
1205 isoamyl alcohol (24:1 ratio) solution was added and the samples again vortexed and centrifuged  
1206 again to separate the layers. At this point the aqueous layer was transferred to a new tube.

1207 To precipitate DNA, to the aqueous layer 10  $\mu\text{g}$  of glycogen (a co-precipitant) and 0.31 times  
1208 the lysate volume of 10.5 M filter sterilized Ammonium Acetate was added. The sample was  
1209 mixed by inverting 5 times, and then 1.31 times the lysate volume of isopropyl alcohol was  
1210 added. Samples were incubated at  $-20^{\circ}\text{C}$  overnight ( $\sim 10$  hours). DNA was pelleted at the

1211 bottom of the tube by spinning at 15,000 g for 60 minutes. The supernatant was decanted off.  
1212 Then the pellet was rinsed with 250 mL -20 °C ethanol and the pellet spun again for 30 minutes.  
1213 The pellet was then air dried in an inverted tube (~2 hours). The pellet was resuspended in 25  
1214 µL of TE (10 mM TRIS-HCl, 1 mM EDTA, pH 8) and incubated at 37 °C for 1-2 hours for the  
1215 DNA to dissolve. DNA concentration was measured using a qubit fluorometer. A sample aliquot  
1216 was then diluted to a final concentration of 2 ng/ul. Samples were then preserved at -80 °C prior  
1217 to further analysis.

### 1218 Amplicon Libraries

1219 Our amplicon libraries leveraged the 515FY-926R primers (Parada et al. 2016) which had  
1220 been amended with overhangs for a final sequence of

1221 Overhang + **515FY**:

1222 5' TCGTCGGCAGCGTCAGATGTGTATAAGAGACAG**GTGYCAGCMGCCGCGG** 3'

1223 Overhang + **926R**:

1224 5' GTCTCGTGGGCTCGGAGATGTGTATAAGAGACAG**CCGYCAATTYMTTTRAGTTT** 3'

1225 Samples were amplified by combining, for a final volume of 25 µL, 1X Accustart Master Mix;  
1226 0.3 mM of each of the forward and reverse primers; 0.5ng/ul of DNA and 5 \* 10<sup>4</sup> of spike-in  
1227 sequence (Genbank Accession LC140931). Samples were amplified in a thermal cycler (BioRad  
1228 T-100) as follows: Samples underwent initial denaturation at 95 °C for 120s. There were then 25  
1229 cycles of denaturation (95 °C \* 45 s) annealing (50 °C \* 45 s), and elongation (68 °C, 90 s).  
1230 Following the amplification cycles, there was a final elongation step of (68 °C, 300 s). Samples  
1231 were then held at 10 °C for less than one hour before being refrigerated at 4 °C. We checked to  
1232 ensure that amplicons appeared in our samples and were the appropriate length by running  
1233 samples on an agarose gel. Samples were then cleaned using AMPure XP beads, following the  
1234 manufacturers' instructions with a bead:sample ratio of 0.8.

1235 Samples were amplified to append unique forward and reverse barcodes and illumina  
1236 adapters:

1237 i7 index primer

1238 5' CAAGCAGAAGACGGCATACGAGAT**XXXXXXXXXX**GTCTCGTGGGCTCGG

1239 i5 index primer

1240 5' AATGATACGGCGACCACCGAGATCTACAC**XXXXXXXXXX**CTCTCTAT

1241 Where bold **Xs** stand in for Illumina i7 index sequences (N701-N729) and i5 index  
1242 sequences (S502-S522).

1243 Samples were again amplified in 25 µL volumes with 1X Accustart master mix, 0.4 mM of  
1244 each primer, and 7 µL of amplified DNA (we do not dilute to a common concentration between  
1245 rounds). Samples were amplified as in round one, but with only five amplification cycles, rather  
1246 than 30.

1247 Fragments were again assessed by agarose gel and cleaned with AMPure XP beads.  
1248 Samples were eluted with TE following amplification. Samples were diluted to a common  
1249 concentration of 5 ng/ul and sent to IMET's Bioanalytical Services laboratory (BASLab) for

1250 sequencing. We found that no samples from station CB5.1 Bottom amplified. Those samples  
1251 were thus re-amplified as part of another batch of samples. Those samples followed the same  
1252 protocol but were eluted in EBT (10 mM Tris, pH 8, 0.1% Tween20) for the final elution step.  
1253 Those samples were sent to UC Davis's Core DNA lab for sequencing. Both sequencing  
1254 facilities ran our samples on an Illumina MiSeq and returned demultiplexed samples to us.  
1255

1256 Two mock community samples of the genomic DNA from 20 organisms, one in which each  
1257 species had even proportions and one in which they had staggered proportions (BEI Resources  
1258 HM-782-D and HM-783D), were run alongside the environmental samples for each run. We also  
1259 ran a "Generous Donor" sample, DNA which we collected from the Horn Point Laboratory Pier  
1260 and which we include in all runs so that they can be cross compared.

### 1261 Amplicon Bioinformatics

1262 To process amplicon sequence data, primers were removed from sequences with Cutadapt  
1263 (Martin 2011). Due to relatively low sequence quality (see Supplemental Results; Amplicon  
1264 Processing), we used the DADA2 `filterandtrim()` algorithm to retain sequences with fewer than  
1265 three errors on the forward read and fewer than five errors on the reverse read, and truncated  
1266 sequences to 230 sequences in the forward and 220 in the reverse direction. DADA2 was then  
1267 used to learn error rates, dereplicate identical sequences, call amplicon sequence variants, and  
1268 to merge forward and reverse reads. Samples from the BasLAB and DNATECH sequence  
1269 libraries were called separately, as recommended by the package developers, and were then  
1270 merged after sequence calling. Chimeric sequences were then removed. Taxonomy was called  
1271 using DADA2's `assignTaxonomy()` function using the Silva database, version 132 (Quast et al.  
1272 2013; Yilmaz et al. 2014), which had been modified by adding the spike in sequences. This  
1273 scheme allowed us to classify bacterial, archaeal and eukaryotic sequences, as well as spike  
1274 sequences.

## 1275 **Supplemental Results**

### 1276 Hydrographic Context

1277 Hydrological conditions can impact the delivery of particles from rivers. The majority (90%)  
1278 of terrestrial suspended solids that enter Chesapeake Bay come from the James, Potomac, and  
1279 Susquehanna Rivers (Figure S1 for locations) (Zhang and Blomquist 2018). The sampled sites  
1280 are primarily influenced by the Susquehanna River because the water flows from North to South  
1281 and all of the sampled sites are north of the James River and only site CB5.5 is south of the  
1282 Potomac River. Discharge at the Conowingo Dam plays a major role in determining of  
1283 suspended sediments load of the water that enters the Bay from the Susquehanna River (Zhang  
1284 et al. 2016) Thus, despite differences in hydrological conditions over the sampling period (i.e.,  
1285 CB5.1 and CB5.5 were sampled at baseflow conditions, CB4.3C and CB3.3C were sampled  
1286 during the rising limb of a storm, and CB3.2 and CB3.1 were sampled on the falling limb of a  
1287 storm; Figure S2A-C), discharge patterns at the Conowingo Dam did not substantially vary over  
1288 the period of sampling (Figure S2A-C) and therefore it is likely that delivery of suspended  
1289 sediments also did not greatly vary over the period of sampling. Additional information about  
1290 physics, chemistry, and the particle size to mass and size to abundance distribution spectra of  
1291 each site, when they were sampled for this study, are described in Dougherty et al. (2021).

1292 Amplicon Processing

1293 Mock community sequencing suggested that overall community structure was broadly in line  
1294 with input communities. In the first sequencing run the even mock community, which contained  
1295 20 species each of which can have more than one 16S sequence, had 25 ASVs that comprised  
1296 at least 1% of the community structure each for a total of 76.8% of the total mock community.  
1297 These reads varied in relative abundance from 9.3% to 1.1%. There were 326 rare ASVs each  
1298 comprising < 1% of the community. In the second run, there were 22 ASVs that comprised at  
1299 least 1% of the community structure ranging in relative abundance from 8.9% to 1.3% each for a  
1300 total of 96% of the overall community, and 189 rare ASVs.

1301 Per sample sequence depth ranged from 7034 reads through 304399 reads (median = 91838 ±  
1302 38019 (median adjusted deviation, MAD)). We use an internal reference standard sample, a  
1303 generous donor DNA sample collected at the HPL pier, as part of every sequencing run that our  
1304 lab does. Sequence quality of this generous donor sample was characteristic of the other  
1305 samples and allowed us to compare sequence quality between runs (Figure S7A-D) while  
1306 ensuring that the community structure was similar between runs. The sequence quality of  
1307 samples from BasLab appeared to drop off more quickly than other projects that we had  
1308 encountered, with quality scores dropping below 30 after about 100 cycles for both the forward  
1309 and reverse reads. In contrast, the samples run by DNATECH appeared to remain above 30  
1310 through 220 bases in the forward direction and 200 cycles in the reverse direction (Figure S7A-  
1311 D).

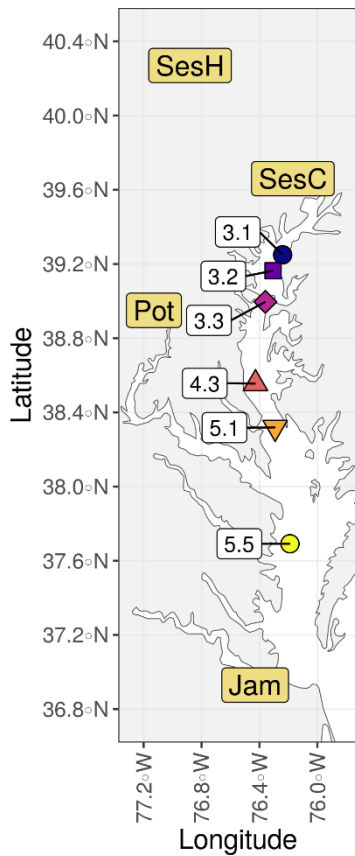
1312 DADA2's chimera checking program suggested that a high fraction of our reads were chimeras  
1313 (range 7.2% - 53.4%; median 33.6% ± 9.4% MAD), in both of our runs. While high fractions of  
1314 detected chimeras are often related to skipping primer trimming steps, we confirmed that this  
1315 step did indeed occur for this analysis. Following all processing steps, we were left with between  
1316 2135 and 142572 reads (median 33803 ± 20198 MAD), including spike in sequences. After  
1317 removing spike in sequences, all samples but three had more at least 9900 reads. The low read  
1318 number samples were CB4.3 Surface 0.2 µm (852 reads); CB3.1 Bottom 500 µm (860 reads)  
1319 CB3.3C Bottom 180 µm (1248 reads).

1320 Microbial community structure data (Table S1), microbial taxonomic information (Table S2), and  
1321 corresponding environmental parameters (Table S3) are available as supplemental tables.

1322

1323

1324 **Supplemental Figures**

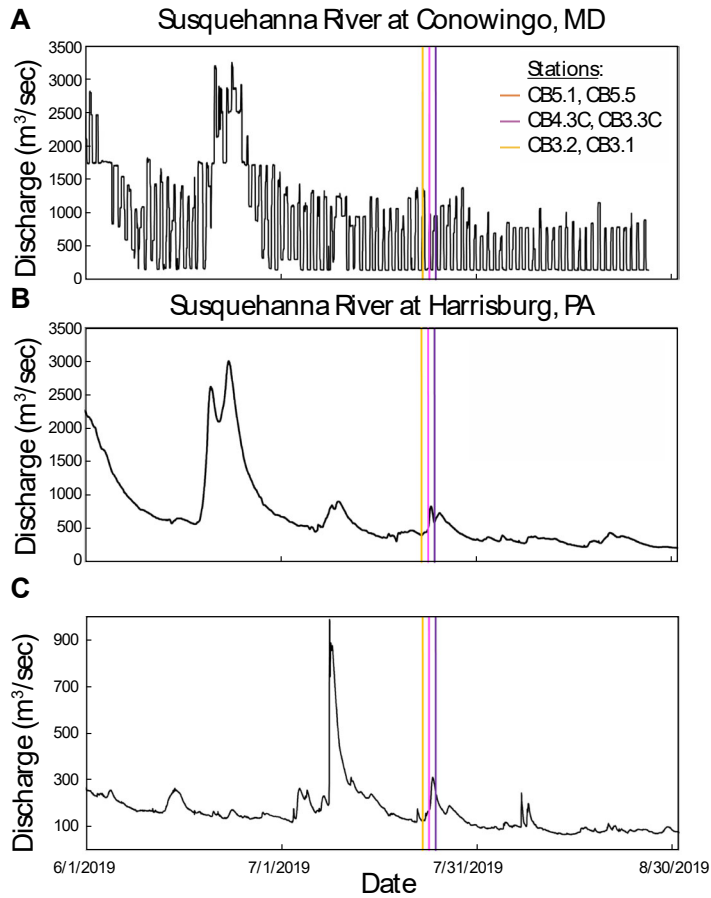


1325

1326 Figure S1. Map of the study area, reflecting not only the station locations shown in Figure 1A,  
1327 but also the locations hydrological stations describing discharge by key rivers into the  
1328 Chesapeake Bay (Figure S2). Each station is labeled in light goldenrod colored rectangles  
1329 (SesH, Sesquihanna River at Harrisburg; SesC, Susquehanna River at Cantonsville; Pot,  
1330 Potomic River near Washington DC). The James river (Jam), mentioned in the main text, is also  
1331 shown.

1332

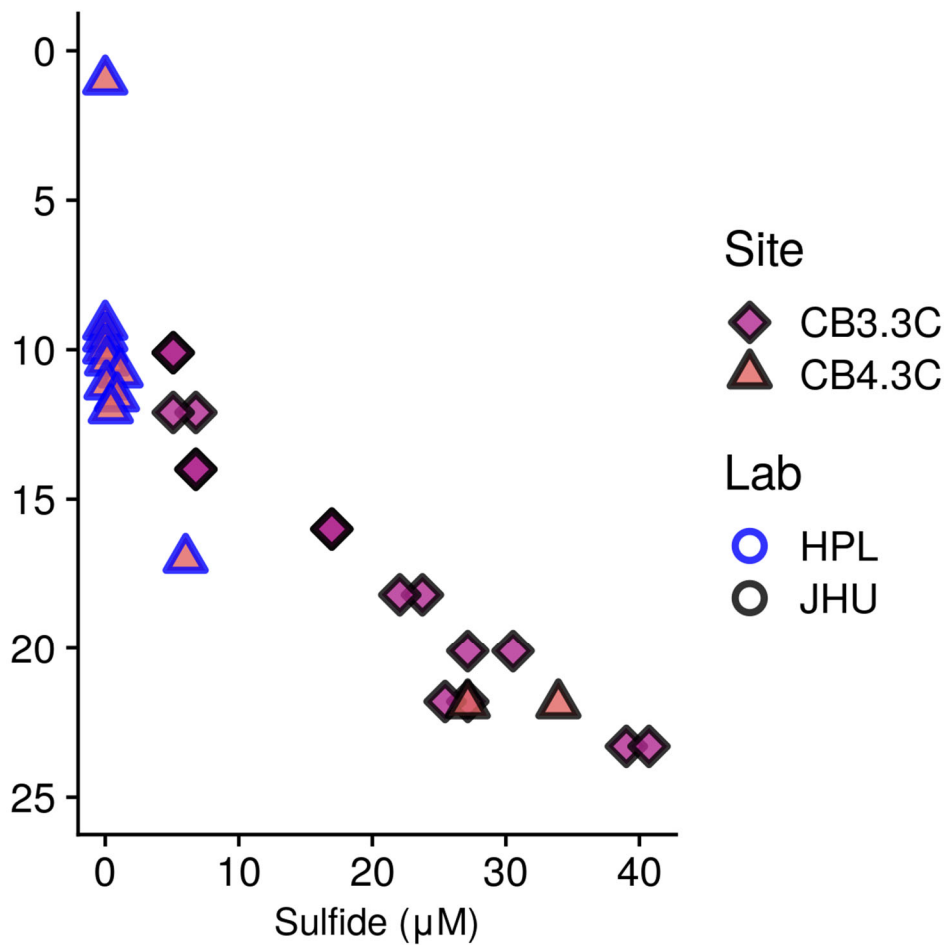
1333



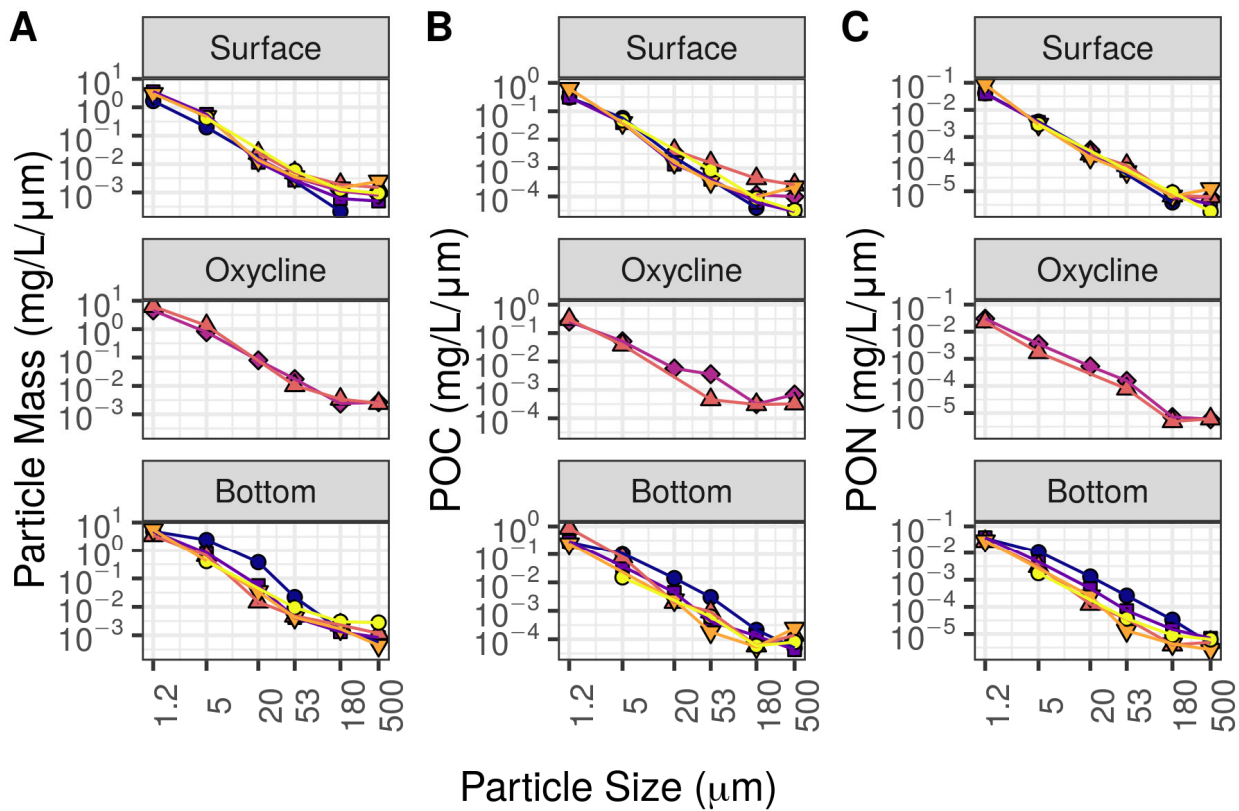
1334

1335 Figure S2. Discharge at United States Geological Survey (USGS) gauges at A) the  
 1336 Susquehanna River at Conowingo, MD (USGS 01578310), B) the Susquehanna River at  
 1337 Harrisburg, PA (USGS 01570500), B) the Susquehanna River at Conowingo, MD (USGS  
 1338 01578310), and C) the Potomac River near Washington, DC (USGS 01646500). Data  
 1339 downloaded from <https://waterdata.usgs.gov/>.

1340

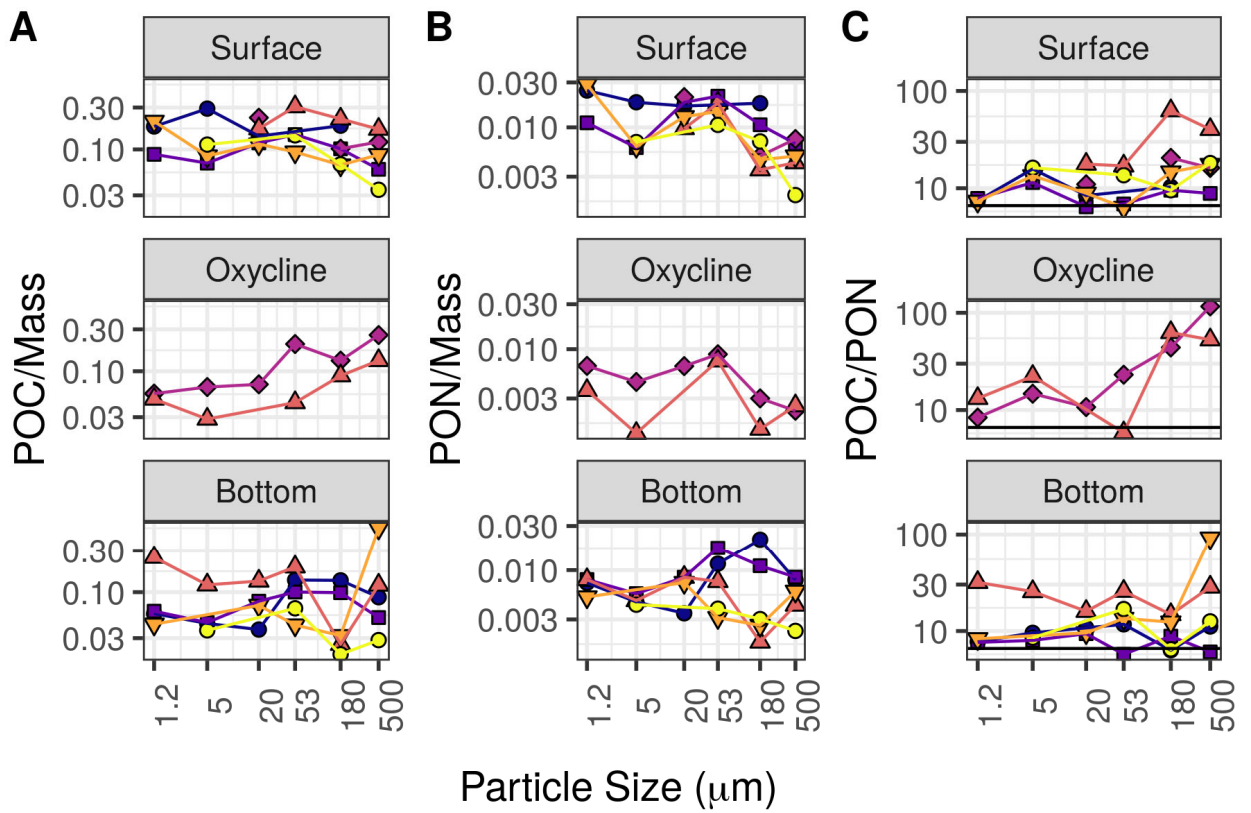


1341  
 1342 Figure S3. Hydrogen sulfide concentrations, measured at stations CB3.3C and CB4.3C. The  
 1343 laboratory which performed the analysis differed between samples and are shown: Horn Point  
 1344 Laboratory (HPL) and Johns Hopkins University (JHU). Sulfide was not measured at any of the  
 1345 other stations, but sulfide was also not detected by smell at any of the other stations.



1346

1347 Figure S4. Particle (A) mass, (B) particulate organic carbon (POC) content and (C)  
 1348 particulate organic nitrogen (PON) content associated with each size fraction, at each measured  
 1349 depth, of each station. Colors and shapes of points correspond to stations as shown in Figure  
 1350 1A and Figure S1.



1351

1352

1353

1354

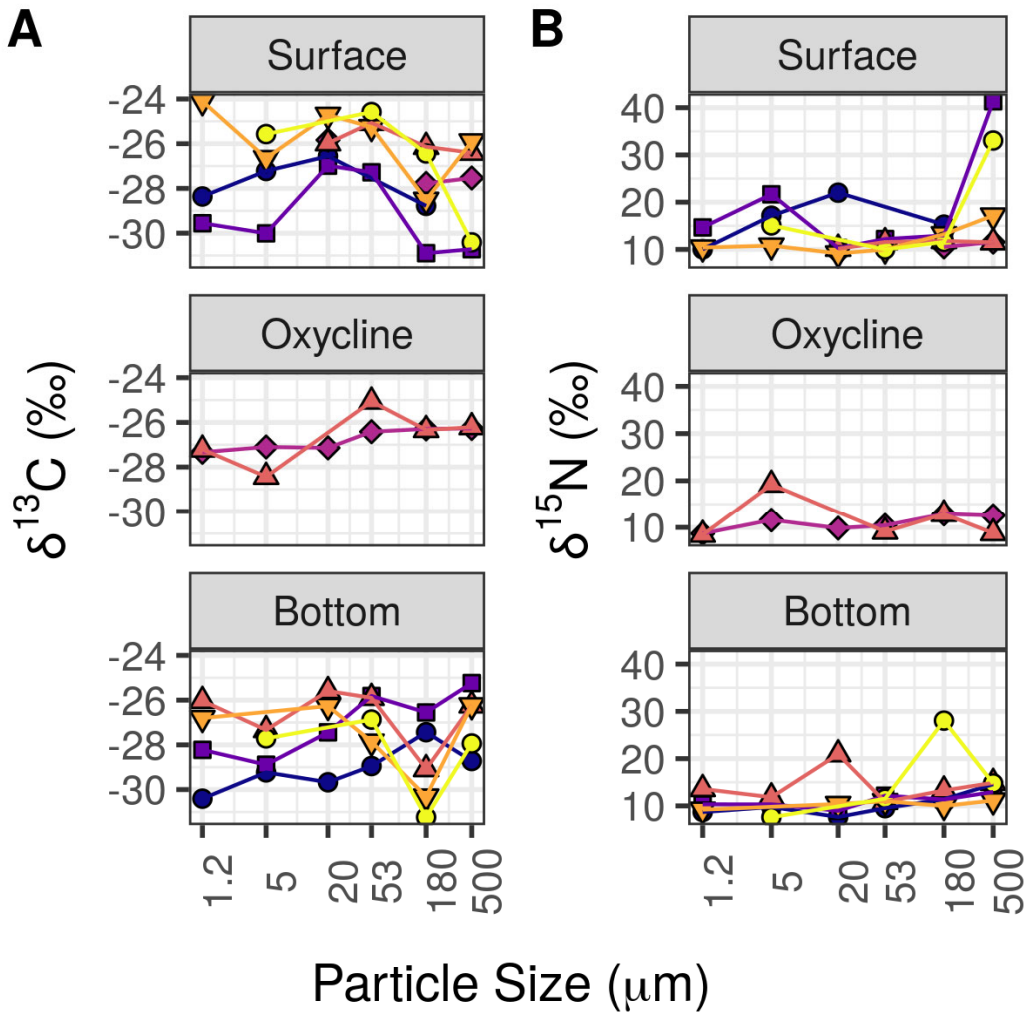
1355

1356

1357

1358

Figure S5. Ratios between the particle characteristics shown in Figure S2, numerators and denominators are all in the same units, and so y axis values are unitless. (A) Particulate organic carbon to mass ratios; (B) Particulate organic nitrogen to mass ratios; (C) Particulate organic carbon to nitrogen ratios. Colors and shapes of points correspond to stations as shown in Figure 1A.



1359

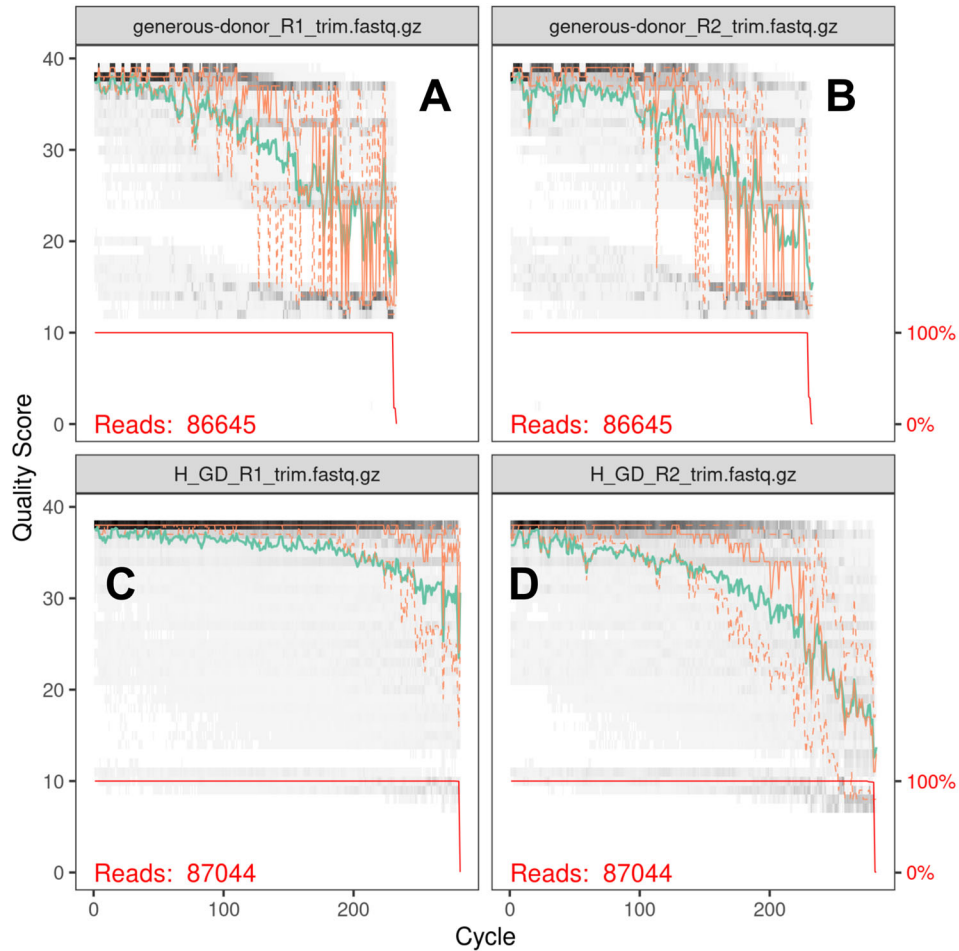
1360

1361

Figure S6. Particulate organic carbon and nitrogen isotopic ratios (A)  $\delta^{13}\text{C}$  and (B)  $\delta^{15}\text{N}$ . Colors and shapes of points correspond to stations as shown in Figure 1A.

1362

1363



1364

1365

1366

1367

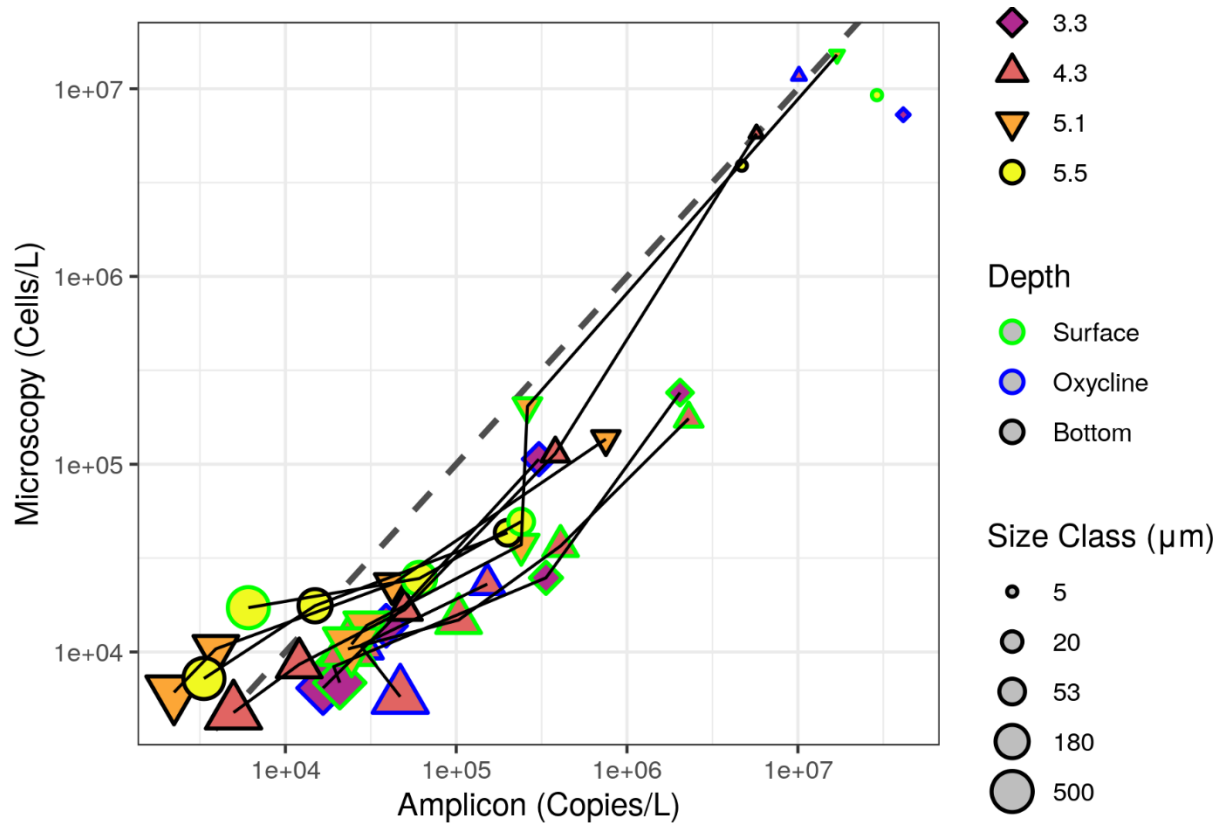
1368

1369

1370

1371

Figure S7. Read quality of generous donor samples (collected at the HPL pier, all size fractions) from our two different sequencing runs. **A-B**, most samples, sequenced by IMET BasLAB, **C-D**, samples from station 5.1 Bottom. Sequenced by UC Davis. **A,C**, Forward read quality. **B,D**, Reverse read quality. This is a standard output by the DADA2 program (Callahan et al. 2016). The heatmap indicates the distribution of scores, as well as a mean best fit score (line). The red line indicates the fraction of samples that are at least a given length.



1372

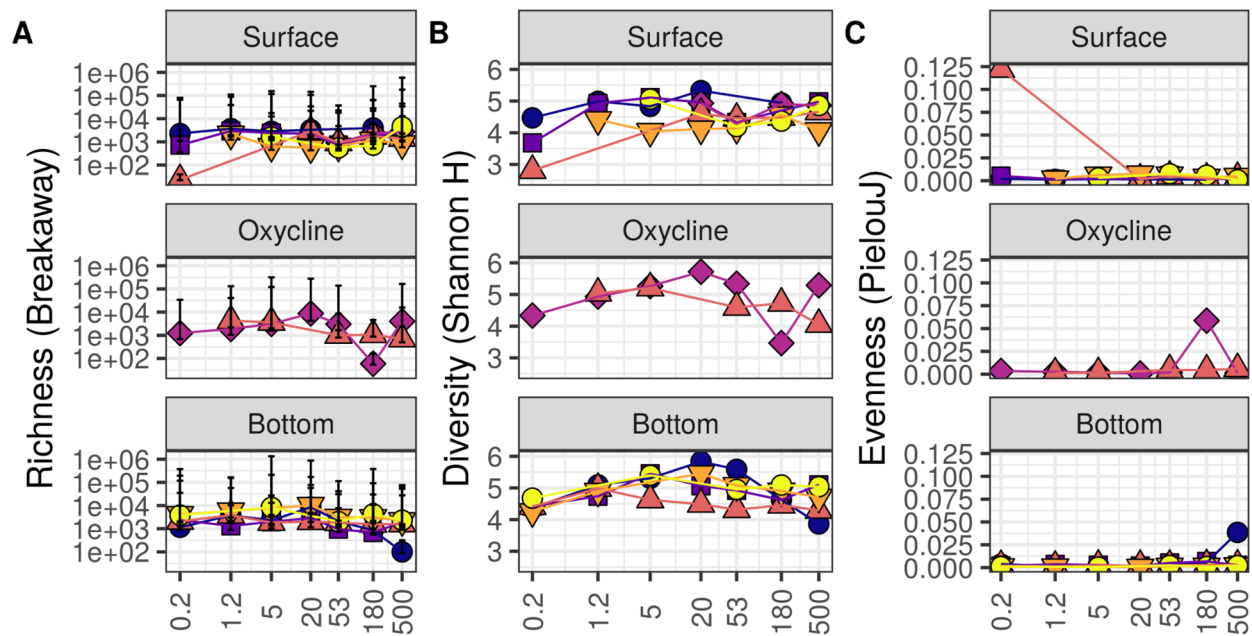
1373 Figure S8. Microscopy-based estimates of microbial abundance compared to amplicon-  
 1374 based estimates. The black diagonal is the one to one line.

1375

1376

1377

1378



1379

1380

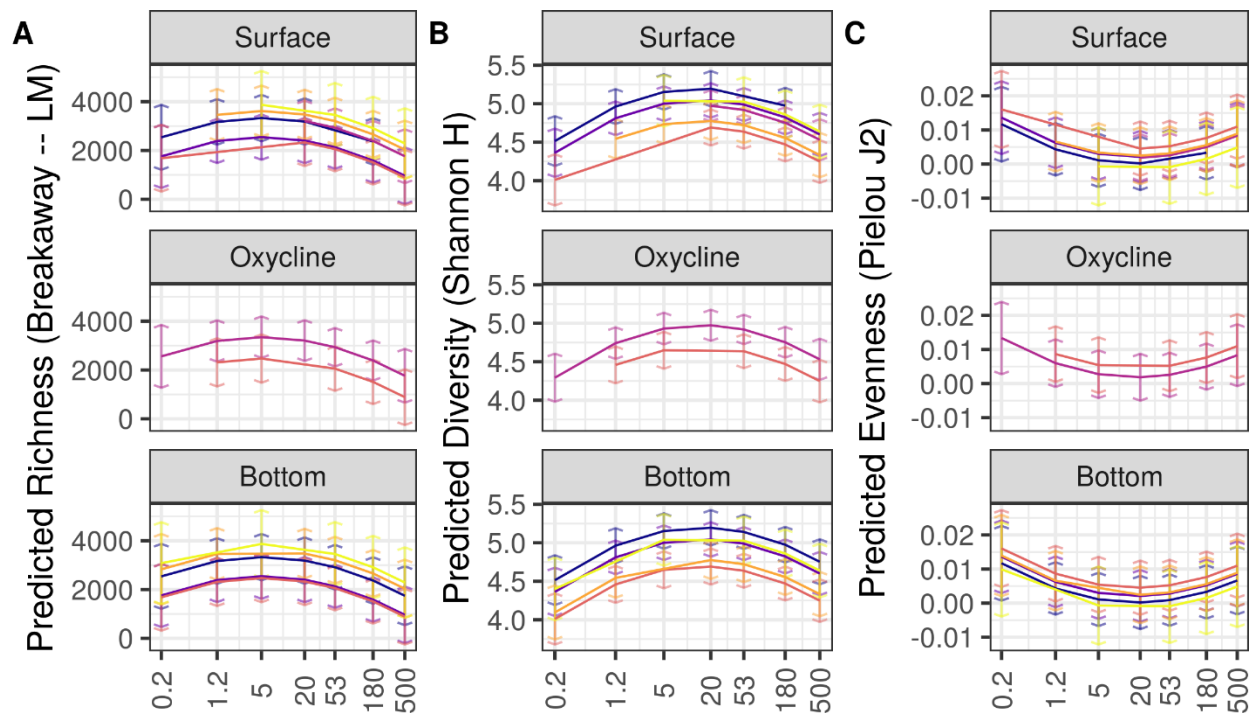
1381

1382

1383

1384

Figure S9. Estimates of **A** richness, **B** Shannon diversity and **C** evenness at each sample. Confidence intervals in **A** correspond to upper and lower bounds specified by the breakaway package. Colors and shapes of points correspond to stations as shown in Figure 1A. Note that richness, but not the other metrics, is on a log scale.



1385

1386

1387

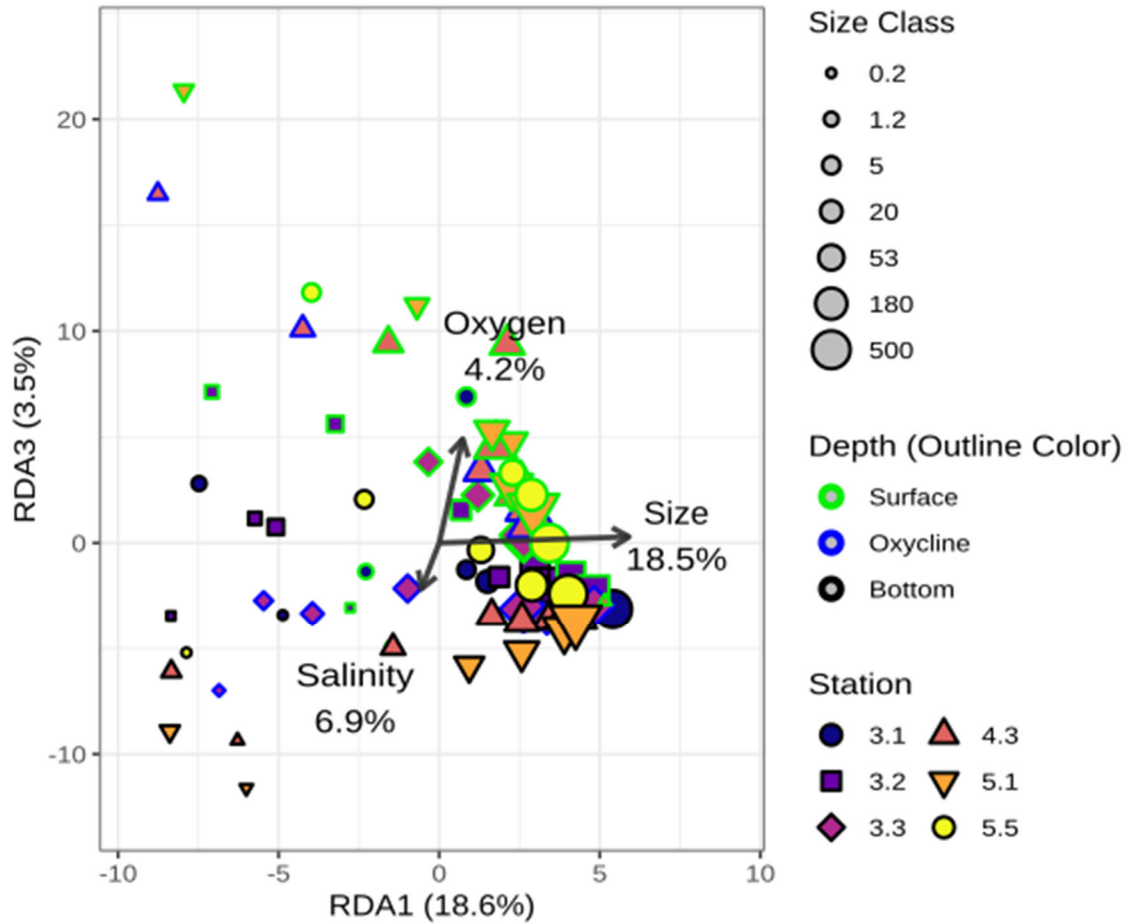
Figure S10. Linear model predicted outputs of **A** richness, **B** Shannon diversity and **C** evenness which show general trends with size and latitude at the surface and bottom of the

1388 water column. Colors of the curves correspond to the colors shown in Figures 1A and S9.  
1389 Confidence intervals are two standard errors of predicted mean values.

1390

1391

1392



1393

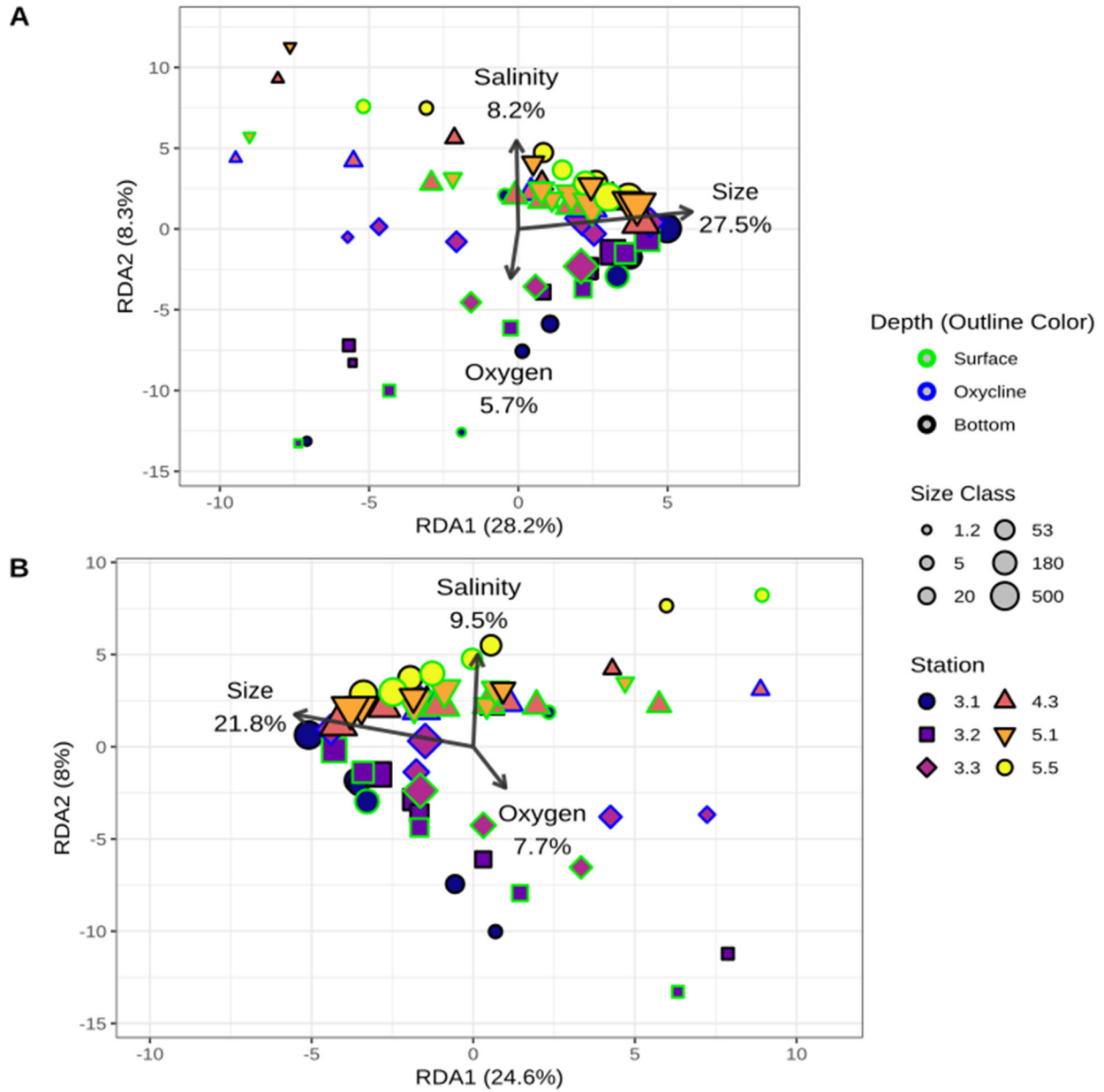
1394 Figure S11. Axes RDA1 and RDA3 of the redundancy analysis shown in Figure 3.

1395

1396

1397

1398

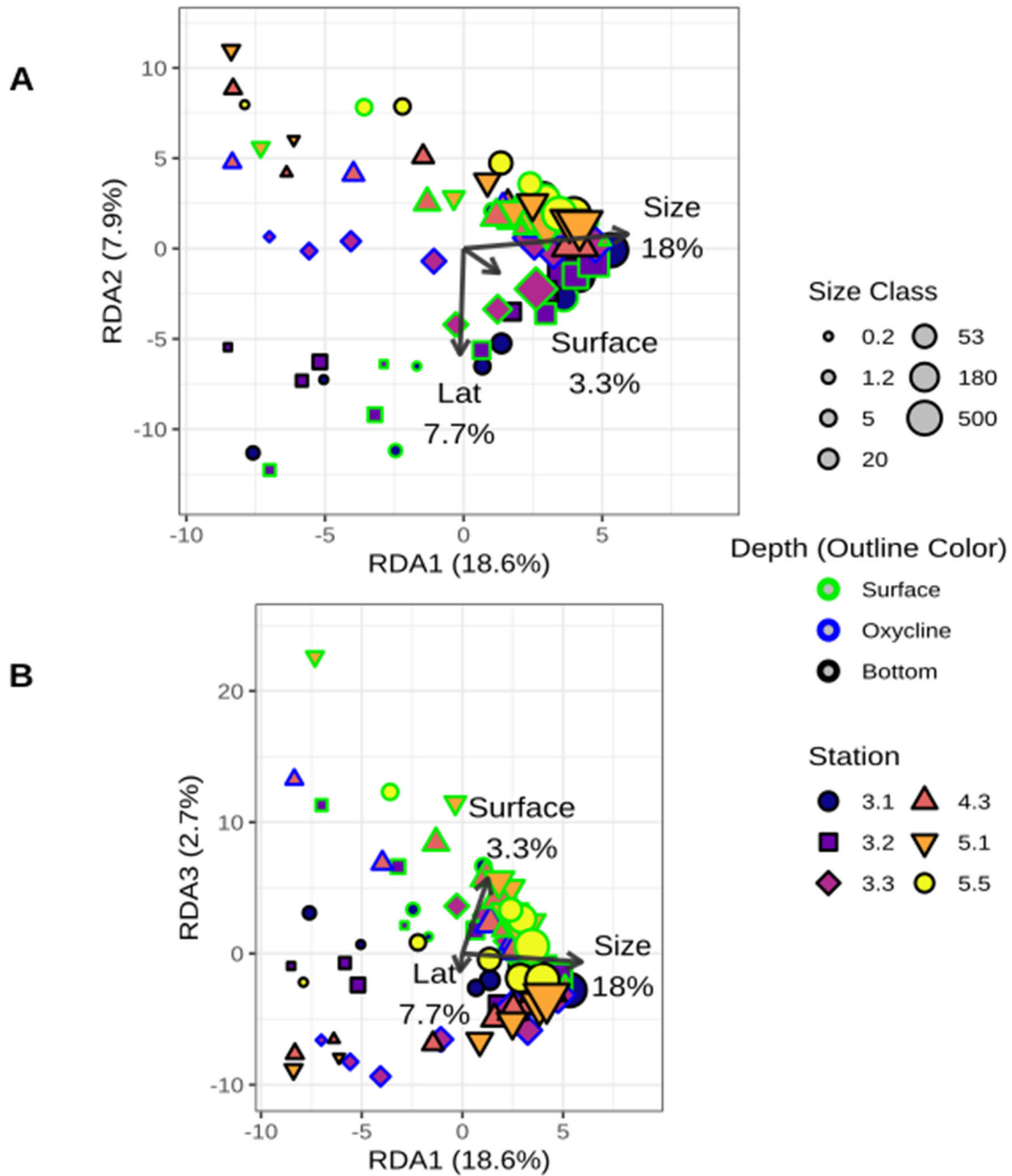


1399

1400 Figure S12. Redundancy analysis of the relationship between Salinity, Oxygen concentration  
 1401 and particle size microbial community structure **(A)** excluding samples from the (0.2 – 1.2  $\mu$ m  
 1402 size classes and **(B)** excluding samples from the 0.2 – 1.2  $\mu$ m and 1.2 – 5  $\mu$ m size classes.

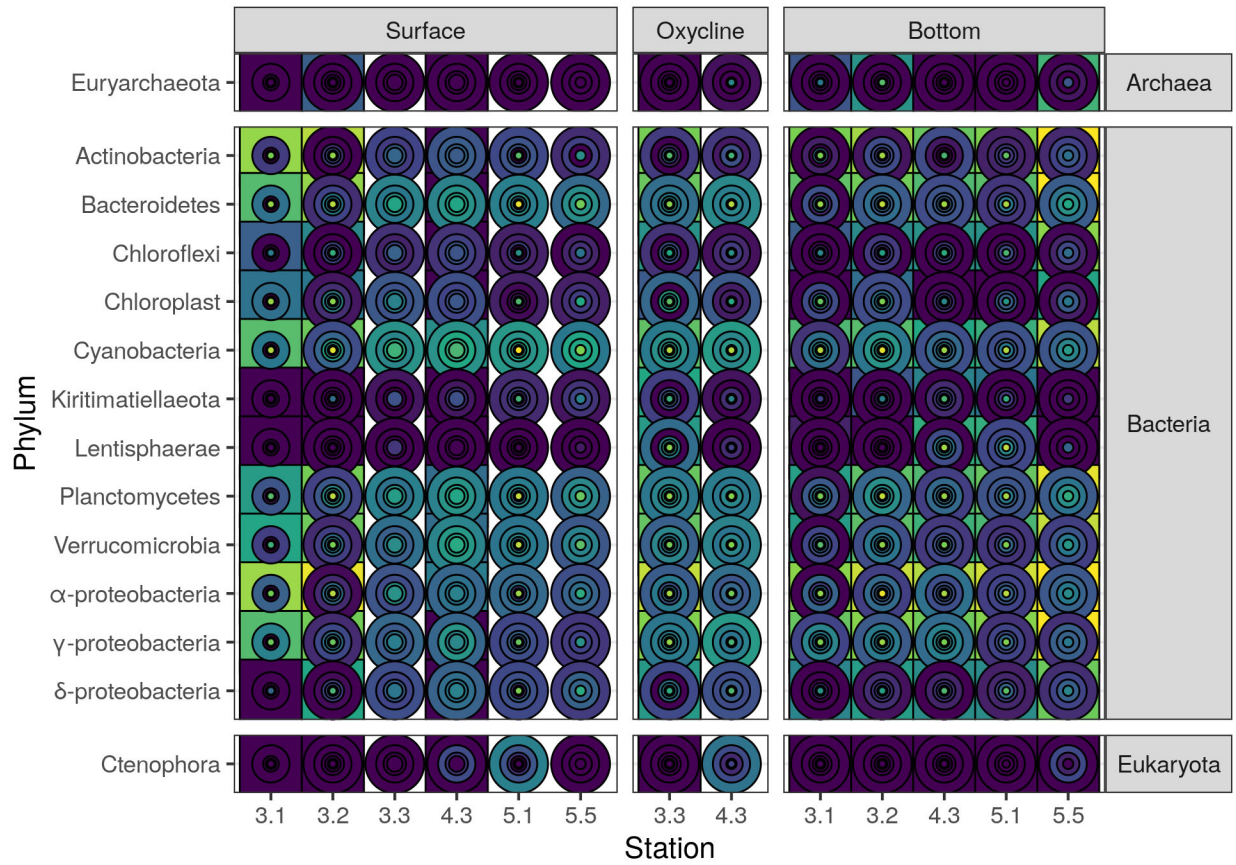
1403

1404



1405

1406 Figure S13. RDA in which latitude and whether the particle was collected at the surface, rather  
 1407 than salinity and oxygen, are used to predict community structure, as in Figures 3 and S11. A.  
 1408 RDA axes 1 and 2. B. RDA axes 1 and 3.



1409

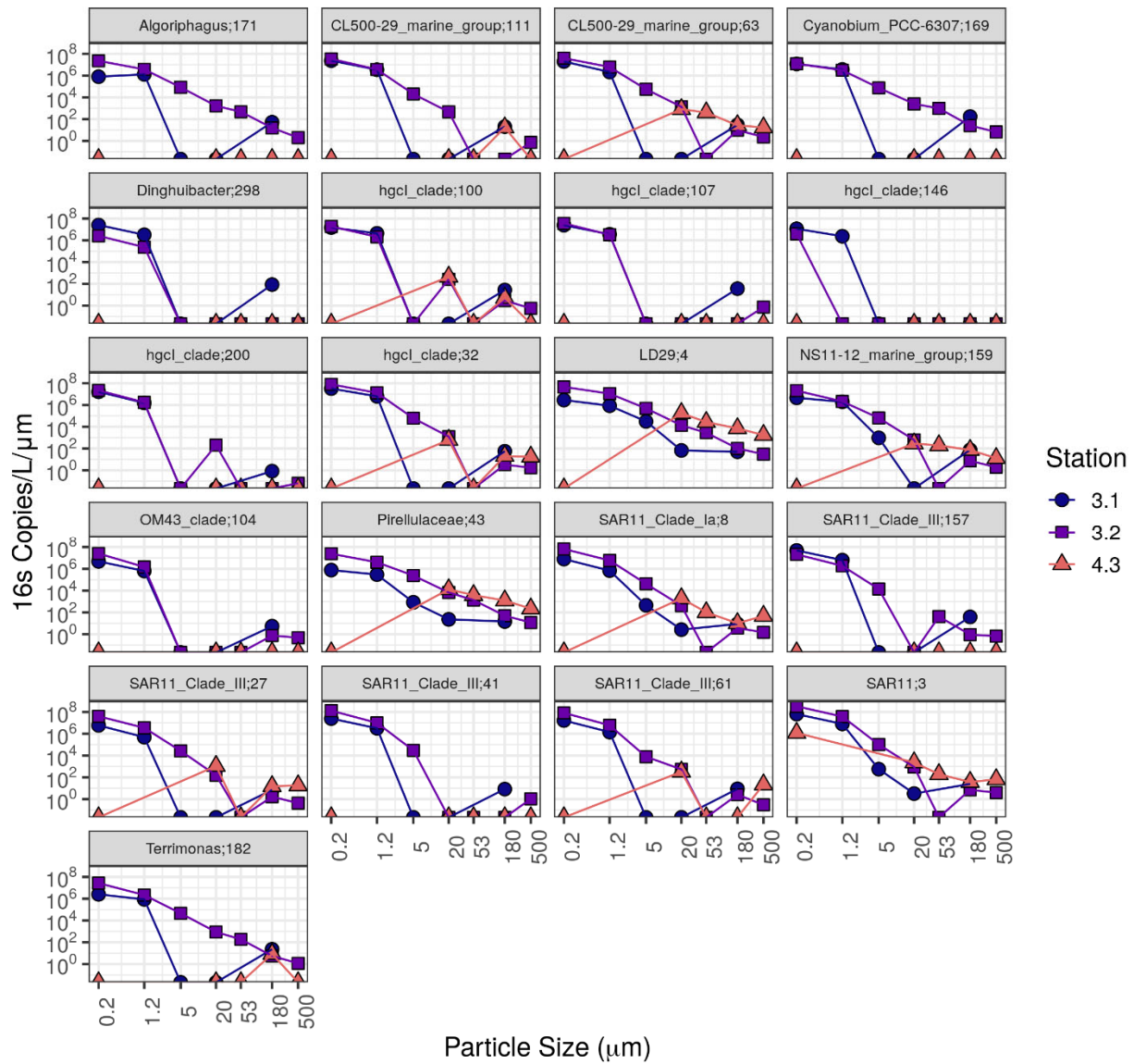
1410

1411 Figure S14. Phylum level abundance of bacteria, normalized to water volume, rather than  
 1412 particle mass.

1413

1414

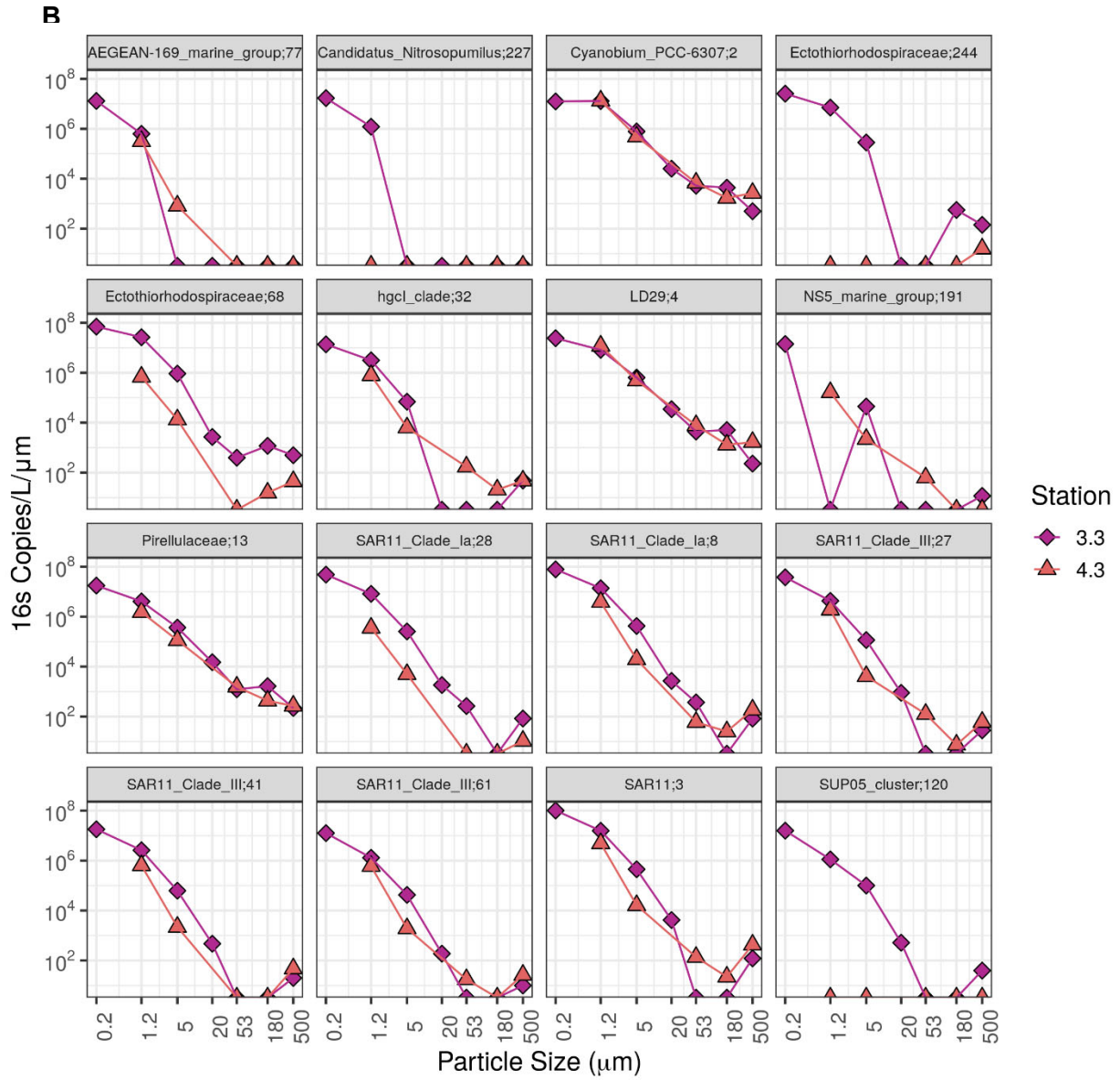
A



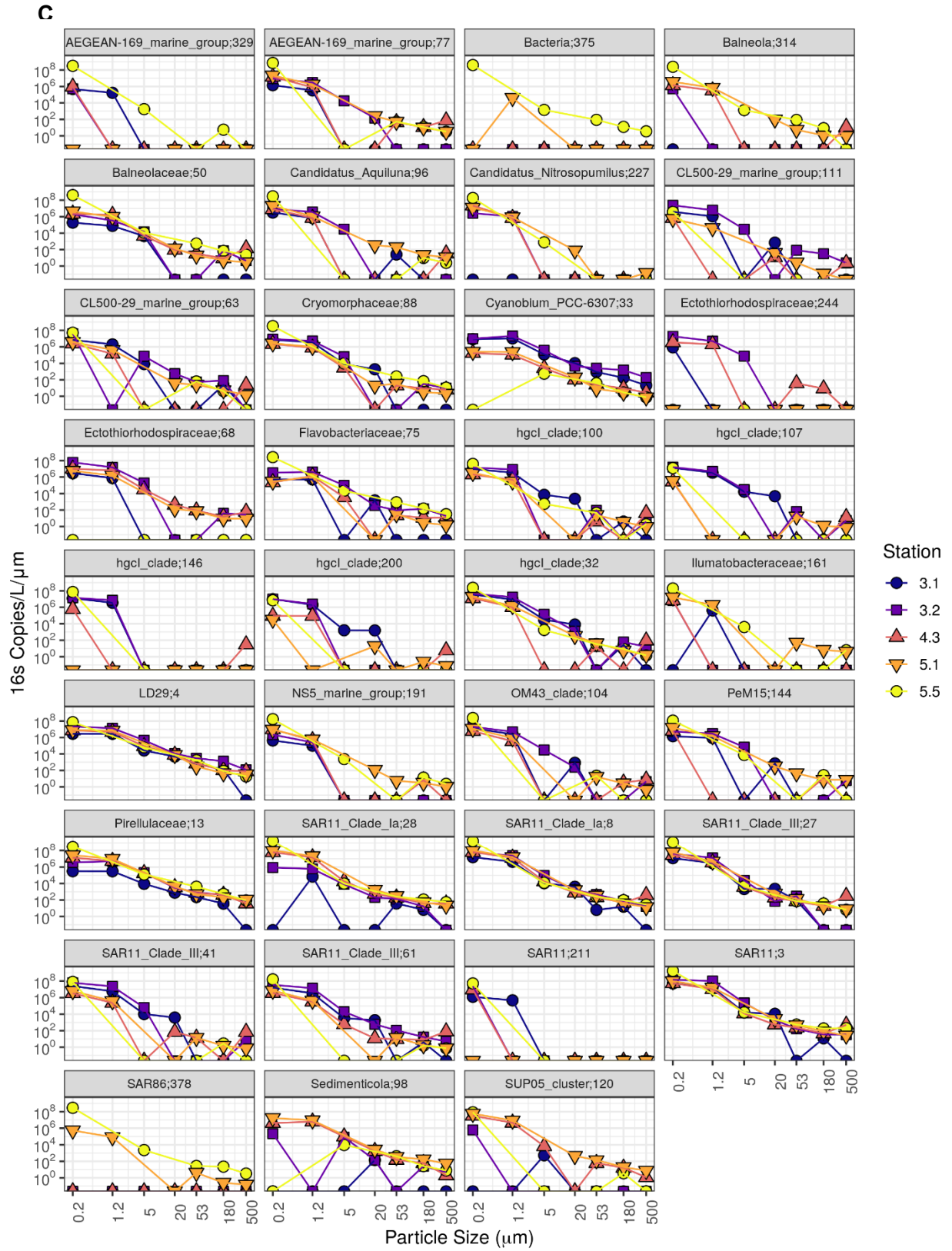
1415

1416

1417



1418



1422 Figure S15. Amplicon sequence variants that comprised at least 1% of the total free-living  
1423 (0.2 – 1.2 µm size fraction) community at at least one station in (A) the surface (B) oxycline and  
1424 (C) the bottom depths. Only station and depth combinations where the free-living bacteria were  
1425 sequenced are shown. All of these ASVs were found to be present in one or more of the larger  
1426 size fractions.

1427

## 1428 Supplemental Tables

1429

1430 **Table S1.** Microbial abundances of each ASV in each location, depth and size fraction. Data  
1431 have been processed to normalize sequence reads by spike concentrations and DNA in the  
1432 environment to produce normalized abundances. Column names as follows

1433 **ASV:** Numbered amplicon sequence variant

1434 **Reads:** Number of reads of that ASV

1435 **ID:** Sample ID of form station-depth-size fraction. For instance, 3-1-B-0-2 is station CB3.1,  
1436 Bottom, Size fraction 0.2-1.2 µm.

1437 **SpikeReads:** Number of reads that taxonomically mapped to the spike-in sequence in each  
1438 sample.

1439 **conversionMultiplier:** DNA per liter \* 10<sup>5</sup> spike in copies / SpikeReads, used for calculating  
1440 concentrations.

1441 **RA:** Relative abundance of the sequence. A value between 0 and 1.

1442 **copiesPerL:** The estimated number of each ASV per L of water in each size-fraction at each  
1443 sample. Calculated by multiplying *Reads* by *conversionMultiplier*

1444 We note that normalized copies per liter can be calculated by dividing *copiesPerL* by *Bin\_Size*,  
1445 and copies per mg of particles can be calculated by dividing *copiesPerL* by *MassperLiter*. This  
1446 table is 6,184,875 lines long and takes 1.4GB of space uncompressed and so is uploaded as its  
1447 own gzip compressed csv file.

1448

1449 **Table S2** Taxonomic information about each amplicon sequence variant.

1450 **Kingdom:Genus** – Taxonomy information about the ASV as returned by DADA2's built in  
1451 classifier and the silva\_nr\_v132 database.

1452 **nASV:** Just the number from the ASV column

1453 **TagLevel:** The finest taxonomic level for which taxonomy is available

1454 **Tag:** The taxonomic identification at TagLevel

1455 **Tag\_ASV:** Tag, appended to nASV. Used when naming ASVs in figures so that the ASV name  
1456 provides information about taxonomy.

1457

1458 **Table S3** Sample information table.

1459 **Station:** Chesapeake bay program station ID. All stations are central bay stations (so 4.3  
1460 means CB 4.3C and so on).

1461 **Size\_Class:** The lower bound of the sample size class. For instance 0.2 means the 0.2 – 1.2  
1462  $\mu\text{m}$  size fraction, while 500 is the  $\geq 500 \mu\text{m}$  size fraction.

1463 **Depth:** Depth category. Surface or Bottom. Station CB 4.3 also has a third Oxycline (Oxy)  
1464 depth.

1465 **Bin\_Size:** The width of the particle size bin ( $\mu\text{m}$ ). Calculated as the upper bound minus the  
1466 lower bound.

1467 **DNALiter:** The amount of DNA extracted from a sample, normalized to volume filtered.

1468 **MassperLiter:** The amount of POM mass measured, normalized to volume filtered. Not  
1469 recorded for the 0.2 – 1.2  $\mu\text{m}$  size bin. This value was previously reported in Dougherty et al.  
1470 (2021).

1471 **ParticlesPerLiter:** Estimated number of particles in a size class, per liter. Measured by LISST  
1472 and summed over all size bins. This value was previously reported in Dougherty et al. (2021).

1473 **Flag:** Some samples did not amplify and/or sequence well. This is especially the case with all  
1474 first run samples from station 5.1B. Only samples where FLAG is false are included here, so  
1475 this is just a column of the word false.  
1476

1477 **Table S4.** Relationships between metrics of alpha diversity (Richness, Shannon Diversity and  
 1478 Evenness) to water salinity, oxygen concentration and particle size. : **Metric:** the alpha diversity  
 1479 metric used. Richness (breakaway – betta) uses the betta function in the breakaway package to  
 1480 carry out the model. All other metrics, use a simple linear model. **Term** indicates the coefficient  
 1481 for which statistics are shown. Shown are estimates and standard errors of coefficients, T  
 1482 values (linear models only) and *p*-values (bolded if  $p < 0.05$ ).

Metric	Term	Estimate	Std. Err.	T	<i>p</i>
Richness (Breakaway – Betta)	Intercept	4.0 x 10 <sup>3</sup>	2.4 x 10 <sup>2</sup>	NA	< <b>0.001</b>
	log <sub>10</sub> (Size Class)	6.5 x 10 <sup>2</sup>	1.4 x 10 <sup>2</sup>	NA	< <b>0.001</b>
	log <sub>10</sub> (Size Class) <sup>2</sup>	-4.0 x 10 <sup>2</sup>	6.2 x 10 <sup>1</sup>	NA	< <b>0.001</b>
	Salinity	-3.7 x 10 <sup>2</sup>	2.1 x 10 <sup>1</sup>	NA	< <b>0.001</b>
	Salinity <sup>2</sup>	1.7 x 10 <sup>1</sup>	1.2 x 10 <sup>0</sup>	NA	< <b>0.001</b>
	log <sub>10</sub> (Oxygen + 0.03)	-8.8 x 10 <sup>1</sup>	3.1 x 10 <sup>2</sup>	NA	0.779
Richness (Breakaway – LM)	Intercept	3.9 x 10 <sup>3</sup>	7.7 x 10 <sup>2</sup>	5.059	< <b>0.001</b>
	log <sub>10</sub> (Size Class)	7.5 x 10 <sup>2</sup>	4.4 x 10 <sup>2</sup>	1.688	0.096
	log <sub>10</sub> (Size Class) <sup>2</sup>	-4.4 x 10 <sup>2</sup>	1.9 x 10 <sup>2</sup>	-2.348	<b>0.022</b>
	Salinity	-4.5 x 10 <sup>2</sup>	1.7 x 10 <sup>2</sup>	-2.610	<b>0.011</b>
	Salinity <sup>2</sup>	2.4 x 10 <sup>1</sup>	9.1 x 10 <sup>0</sup>	2.586	<b>0.012</b>
	log <sub>10</sub> (Oxygen + 0.03)	4.4 x 10 <sup>2</sup>	7.6 x 10 <sup>2</sup>	0.574	0.568
Diversity (Shannon H)	Intercept	5.2 x 10 <sup>0</sup>	2.0 x 10 <sup>-1</sup>	26.613	< <b>0.001</b>
	log <sub>10</sub> (Size Class)	5.0 x 10 <sup>-1</sup>	1.1 x 10 <sup>-1</sup>	4.461	< <b>0.001</b>
	log <sub>10</sub> (Size Class) <sup>2</sup>	-2.1 x 10 <sup>-1</sup>	4.8 x 10 <sup>-2</sup>	-4.278	< <b>0.001</b>
	Salinity	-9.5 x 10 <sup>-2</sup>	4.4 x 10 <sup>-2</sup>	-2.175	<b>0.033</b>
	Salinity <sup>2</sup>	3.2 x 10 <sup>-3</sup>	2.3 x 10 <sup>-3</sup>	1.386	0.170
	log <sub>10</sub> (Oxygen + 0.03)	-1.4 x 10 <sup>-1</sup>	1.9 x 10 <sup>-1</sup>	-0.738	0.463

Evenness (Pielou J)	Intercept	$6.1 \times 10^{-4}$	$6.6 \times 10^{-3}$	0.092	0.927
	$\log_{10}(\text{Size Class})$	$-8.3 \times 10^{-3}$	$3.8 \times 10^{-3}$	-2.182	<b>0.033</b>
	$\log_{10}(\text{Size Class})^2$	$3.2 \times 10^{-3}$	$1.6 \times 10^{-3}$	1.965	0.053
	Salinity	$1.0 \times 10^{-3}$	$1.5 \times 10^{-3}$	0.687	0.494
	Salinity <sup>2</sup>	$-3.4 \times 10^{-5}$	$7.8 \times 10^{-5}$	-0.432	0.667
	$\log_{10}(\text{Oxygen} + 0.03)$	$4.8 \times 10^{-3}$	$6.5 \times 10^{-3}$	0.738	0.463

1483

1484

1485 **Table S5.** Coefficients of an ANOVA like permutation test of the RDA analysis coefficients  
 1486 describing the relationship between water salinity, oxygen concentration and particle size and  
 1487 overall microbial community structure. Three Datasets are run: All (Figure S11), which includes  
 1488 all size classes. Particle associated (Figure S12A) which exclude the free-living 0.2 – 1.2  $\mu\text{m}$   
 1489 size class samples and  $\geq 5$  Micron Particles which exclude both the 0.2– 1.2  $\mu\text{m}$  and 1.2 – 5  $\mu\text{m}$   
 1490 size classes. **Term** indicates the coefficient for which statistics are shown. **DF** corresponds to  
 1491 degrees of freedom. **Variance** is the total variance explained by each coefficient. **% Variance** is  
 1492 the variance divided by total variance. **T** is the relevant statistic for the test and **p** is the p-value  
 1493 of that statistic.

1494

1495

<b>Dataset</b>	<b>Term</b>	<b>DF</b>	<b>Variance</b>	<b>% Variance</b>	<b>T</b>	<b>p</b>
All	Salinity	1	745	6.9%	7.0	< <b>0.001</b>
	$\log_{10}(\text{Oxygen} + 0.03)$	1	458	4.2%	4.3	< <b>0.001</b>
	$\log_{10}(\text{Size Class})$	1	2002	18.5%	18.7	< <b>0.001</b>
	Residual	71	7613	70.4%		
Particle Associated	Salinity	1	781	8.2%	8.7	< <b>0.001</b>
	$\log_{10}(\text{Oxygen} + 0.03)$	1	546	5.7%	6.1	< <b>0.001</b>
	$\log_{10}(\text{Size Class})$	1	2616	27.5%	29.1	< <b>0.001</b>
	Residual	62	5567	58.5%		
$\geq 5$ Micron Particles	Salinity	1	534	9.5%	8.2	< <b>0.001</b>
	$\log_{10}(\text{Oxygen} + 0.03)$	1	432	7.7%	6.6	< <b>0.001</b>
	$\log_{10}(\text{Size Class})$	1	1229	21.8%	18.9	< <b>0.001</b>
	Residual	53	3445	61.1%		

1496

1497